

Article

Protective Effects of *Aquilaria agallocha* and *Aquilaria malaccensis* Edible Plant Extracts against Lung Cancer, Inflammation, and Oxidative Stress—*In Silico* and *In Vitro* Study

Jinnatun Nahar ^{1,†}, Vinothini Boopathi ^{1,†}, Esrat Jahan Rupa ¹, Muhammad Awais ¹,
Anjali Kariyath Valappil ², Md Niaj Morshed ¹, Mohanapriya Murugesan ¹, Reshmi Akter ¹, Dong Uk Yang ³,
Ramya Mathiyalagan ¹, Deok Chun Yang ^{1,4,*} and Seok-Kyu Jung ^{5,*}

- ¹ Graduate School of Biotechnology, College of Life Sciences, Kyung Hee University, Yongin 17104, Gyeonggi-do, Republic of Korea; jinnatunnaharbph@gmail.com (J.N.); vinothini9327@gmail.com (V.B.); eshratrupa91@gmail.com (E.J.R.); awaiskazmi@khu.ac.kr (M.A.); niajmorshed96@khu.ac.kr (M.N.M.); priyabuddy44@gmail.com (M.M.); reshmiakterbph57@gmail.com (R.A.); ramyabinfo@gmail.com (R.M.)
- ² Department of Biopharmaceutical Biotechnology, College of Life Sciences, Kyung Hee University, Yongin-si 17104, Gyeonggi-do, Republic of Korea; anjalikv111@gmail.com
- ³ Hanbangbio Inc., Yongin-si 17104, Gyeonggi-do, Republic of Korea; rudckfeo23@naver.com
- ⁴ Department of Oriental Medicinal Biotechnology, College of Life Sciences, Kyung Hee University, Yongin-si 17104, Gyeonggi-do, Republic of Korea
- ⁵ Department of Horticulture, Kongju National University, Yesan 32439, Chungcheongnam-do, Republic of Korea
- * Correspondence: dcyang@khu.ac.kr (D.C.Y.); jungsk@kongju.ac.kr (S.-K.J.)
- † These authors contributed equally to this work.



Citation: Nahar, J.; Boopathi, V.; Rupa, E.J.; Awais, M.; Valappil, A.K.; Morshed, M.N.; Murugesan, M.; Akter, R.; Yang, D.U.; Mathiyalagan, R.; et al. Protective Effects of *Aquilaria agallocha* and *Aquilaria malaccensis* Edible Plant Extracts against Lung Cancer, Inflammation, and Oxidative Stress—*In Silico* and *In Vitro* Study. *Appl. Sci.* **2023**, *13*, 6321. <https://doi.org/10.3390/app13106321>

Academic Editors: Anna Olejnik and Katarzyna Kowalska

Received: 18 April 2023

Revised: 16 May 2023

Accepted: 17 May 2023

Published: 22 May 2023



Copyright: © 2023 by the authors. Licensee MDPI, Basel, Switzerland. This article is an open access article distributed under the terms and conditions of the Creative Commons Attribution (CC BY) license (<https://creativecommons.org/licenses/by/4.0/>).

Abstract: The family Thymelaeaceae, which includes huge evergreen trees that are sparsely distributed in tropical rainforests, includes the genus *Aquilaria*. Numerous medical conditions, including inflammation, cancer, and oxidative stress have been traditionally treated using *Aquilaria agallocha* and *Aquilaria malaccensis*. In this study, we evaluated *in silico* and biological activity with *A. agallocha* and *A. malaccensis* sample for more conformation. Raw 264.7 macrophage cells and HacaT cells were used, together with the MTT, ROS, NO, and wound healing assays, to investigate the possible cytotoxicity in A549 lung cancer. Thus, *A. agallocha* and *A. malaccensis* showed significant cytotoxicity against A549 cancer cells at 1000 µg/mL. Furthermore, we observed an elevated ROS level in cancer cells. The wound healing assay showed cancer cell inhibition activity. While *BCL-2* decreased in the intrinsic route, *p53*, *Bax*, *Caspase 3*, and *Caspase 9* were elevated by A.A and A.M. Additionally, we have also conducted an *in silico* evaluation followed by molecular dynamics (MD) simulations, along with ADMET and biological activity prediction to further validate the experimental results. In normal cells, both samples showed less toxicity at 1000 µg/mL and suppressed the LPS-treated NO and ROS levels against the inflammation. Additionally, A.A and A.M suppressed the pro-inflammatory gene expression of *COX-2*, *iNOS*, *TNF-α*, *IL-6*, and *IL-8* in RAW 264.7 cells. On the other hand, A.A and A.M extract effectively suppressed oxidative stress by increasing the antioxidative gene expression in H₂O₂-induced HaCat cells at 50 µg/mL. This study revealed that the plant extracts from *A. agallocha* and *A. malaccensis* could exert a cytotoxic effect on lung adenocarcinoma cells through the activation of an intrinsic signaling pathway. Moreover, it could be a potential source of anti-inflammatory, antioxidant, and anti-cancer agents after consideration of *in vivo* and clinical studies.

Keywords: *Aquilaria agallocha*; *Aquilaria malaccensis*; molecular docking; anti-cancer; anti-inflammation; antioxidant

1. Introduction

Inflammation is the body's natural defense mechanism against pathogens, manifested as a cellular injury that releases immune system mediators. Redness (rubor), swelling (tumor), heat (calor), and hyperalgesia (dolor), which are considered the "cardinal signs of inflammation," appear as an immediate reaction to a local inflammatory stimulus. [1]. Inflammatory substances such as bradykinin, serotonin, histamine, prostaglandins, leukotrienes, and nitric oxide that might come from local sources or cells that penetrate the site of the assault, cause these symptoms [2]. As a result, therapy can successfully treat inflammation by reducing the overproduction of pro-inflammatory mediators. Additionally, it contributes to the pathogenesis of numerous human disorders, including the growth and spread of cancer. Global Cancer Statistics 2020 states that there are 19.3 million new instances and nearly 10 million deaths from cancer in the whole world, making it a dreadful, fatal disease with a higher mortality rate. Lung cancer continues to be the leading cause of cancer-related death, with approximately 1.8 million deaths and 2.20 million cases reported every year [3]. Most lung cancers, or 85% with minimal therapeutic activity, are non-small cell lung cancers (NSCLC) [4]. Today, cancer is treated with various conventional drugs, including chemotherapies, radiation, and surgery. Although combining several therapies enhances the likelihood that cancer patients will survive for a more extended period, the overall outcome is still unsatisfactory due to the adverse effects of drug resistance [5,6]. To improve lung cancer patient survival by minimizing or eliminating negative effects, it is urgently necessary to expand novel therapy techniques. Natural plants have distinct efficacy, safety, and economic effects on conditions. Moreover, much research has found that natural plants have anti-cancer and anti-inflammatory activity [7,8]. Almost every country has a strong acceptance of herbal medications. Additionally, a large traditional herbal medicine was used in China's strategy to prevent and cure severe acute respiratory syndrome (SARS) [9]. In some African countries, up to 80% of the population uses herbal remedies as their primary form of treatment. Therefore, the World Health Organization advises employing herbal remedies in conventional medicine for cancer treatment, degenerative disease prevention, and public health maintenance [10–12]. Large evergreen trees of the genus *Aquilaria*, members of the Thymelaeaceae family, are widespread across Indonesia and sporadically growing in tropical rainforests. This genus is most well-known for being the primary source of agarwood, a resinous wood found inside heartwood that the tree produces as a self-healing mechanism when it is wounded or infected by insects, microbes, or humanmade stimuli [13]. Agarwood, also known as aloeswood or eaglewood, is a resinous wood that is produced by the *Aquilaria*, *Gonystylus*, and *Gyrinops* trees. It is often dense, heavy, and fragrant. Agarwood is produced through a lengthy process and is only found in a small portion of *Aquilaria* trees; as a result, it is valued for being uncommon and precious [14]. The traditional use of agarwood from *aquilaria* trees includes the treatment of inflammatory diseases such as rheumatism, arthritis, and asthma as well as its analgesic, sedative, antibacterial, and anti-diabetic properties [15–19]. Initially, Grewin, Aquillochin, Norketoagarofuran, Jinkohol, 10-epi-gamma-eudesmol, Baimuxinal, Gmelofuran, Agarospirol, Agarol, Kusunol, Beta-Agarofuran, Calarene, Alpha-Agarofuran, Hinesol, and Jinkohol II were the first fifteen compounds we chose for *in silico* studies. The oil extract has been observed to contain the fifteen chemicals listed above in the majority, and it may be because of these compounds that the oil has strong anti-inflammatory and antioxidative stress properties [20]. It is essential for the development of natural products as medicines to understand the molecular interactions between the chemicals and the macromolecules, as well as to predict their biological activity and ADMET. Hence, we have predicted the best compounds' biological activity and ADMET properties, followed by molecular docking and MD simulation studies. The compound Grewin and others showed promising results, with all the proteins used in the docking studies affirming the anti-cancer and anti-inflammatory activity. Furthermore, Grewin interacted with the active binding sites of *BCL-2* with a suitable binding mode similar to that of the control drug BDA-366. Therefore, we have incorporated it into the molecular dynamics study, which assesses the

selected compound and protein complexes' structural stability, conformational changes, and protein movements.

Reactive oxygen species are extracellular mediators that promote a number of signaling pathways, such as the development and progression of cancer [21]. ROS are created excessively through mitochondria in cancer cells, which contributes to the disease's progression by altering gene expression, causing genomic instability, and participating actively in signaling networks [22]. Additionally, the regulation of mitochondrial processes involved in the genesis and homeostasis of cancer is regulated by mitochondrial ROS [23]. Previous studies showed that ROS could control the *p53/Bax/BCL-2* signaling pathway, which controls cancer growth and apoptosis [24–26]. The antioxidant system is a vital defensive mechanism against oxidative harm to cells [27]. The antioxidant system includes extrinsic antioxidant substances that reduce the toxicity of free radicals as well as intrinsic enzymes such as superoxide dismutase (SOD), catalase (CAT), glutathione peroxidase (GPx), and glutathione S transferase (GST), among others [28]. Inflammation that is chronic and causes damage to healthy tissue is also brought on by an overactive inflammatory response. Several mediators, *IL-6*, *IL-8*, *TNF- α* , and *COX-2* [29], are the critical mediators of skin inflammation responses. In experimental models of inflammation, lipopolysaccharide (LPS) is a frequent endotoxin. It is notable that activated macrophages initiate the inflammatory response to chronic inflammation by creating increased nitric oxide, reactive oxygen species, and inflammatory cytokines such as tumor necrosis factor-alpha (*TNF- α*) and interleukin-6 (*IL-6*) [30,31]. Therefore, the natural antioxidant enzymes are stimulated by AA and AM, which suggests that they have antioxidant capabilities.

However, to our understanding, the anti-cancer and anti-inflammatory properties of the *Aquilaria agallocha* and *Aquilaria malaccensis* extract have not yet been thoroughly investigated. Therefore, in the current study, we aim to investigate the anti-cancer and anti-inflammatory effects of *A. agallocha* and *A. malaccensis* in RAW 264.7 macrophages and A549 cancer cells, along with additional *in silico* and *in vitro* analysis. Additionally, *an in vitro* investigation utilizing RAW 264.7 macrophages and A549 cells suggested that the *p53/BCL-2* signaling pathway may be involved in the production of pro-cytokines linked to inflammation.

2. Materials and Methods

2.1. Chemical

Aquilaria agallocha and *Aquilaria malaccensis* samples were provided by Nature Garden, South Korea. The lung cancer cell line (A549) and Raw 264.7 murine macrophage cells utilized in this study were given by the Korean Cell Line Bank (KCLB, Jongno-gu, Seoul-03080, Republic of Korea). Gen DEPOT (Barker, TX, USA) supplied the penicillin-streptomycin solution and fetal bovine serum. Dulbecco's Modified Eagle's Medium and 3-(4, 5-dimethylthiazol-2-yl)-2,5-diphenyltetrazolium bromide, Life Technologies, Eugene, OR, USA, were provided by Gibco (Waltham, MA, USA).

2.2. Preparation of *A. agallocha* and *A. malaccensis* Extract

The samples were collected and dried in a L'EQUIP dehydrator at 35 °C for 20 h after being cleaned with distilled water. After drying, the samples were made into a fine powder with the help of a household grinder. Next, the sample was weighed 1 g, dissolved in 60% ethanol, and sonicated for 140 min to extract bioactive compounds. After the sonication, a rotary evaporator was used to obtain a crude extract, and finally, 20 mg/mL of crude extract was made by dissolving it with EtOH.

2.3. Preparation of Overall Phenolic and Flavonoid Content

To evaluate the total phenolic content assay, the Folin–Ciocalteu (FC) method was applied with gallic acid as standard (0.01–0.6 $\mu\text{g/mL}$) by the minor adjustment of the previously published literature [32]. In short, 30 μL of ethanol extract (1000 ppm) aliquoted with 150 μL of 10% 2N FC reagent was thoroughly vortexed and kept for 5 min. After that,

we added 160 μL of 7.5% Na_2CO_3 and left it for 60 min in a dark place. The absorbance was observed at a wavelength of 715 nm using an ELISA reader. Then, the total flavonoid content test was performed by the AlCl_3 colorimetric method using rutin as standard (0.025–0.8 $\mu\text{g}/\text{mL}$) [33]. Briefly, to provide a sample test (a mixture of 50 μL of plant extract, 150 μL distilled water, 10 μL of 1M CH_3COOK , 10 μL of 10% AlCl_3 , and another 280 μL distilled water), homogenization and incubation (30 min) of the sample were performed. The absorbance was identified at a wavelength of 415 nm.

2.4. Determination of DPPH Radical Scavenging Activity

According to a previous research paper with short modification [34], 20 μL plant extract and 180 μL 0.2 mM DPPH radical solution (formulated with 100% ethanol) were mixed. To get a better reaction, the mixture was kept at room temperature for 30 min in the dark. As a blank, 1 mL of 100% ethanol was included. The control was 180 μL of DPPH and 20 μL of the solvent of the sample. After the incubation, the absorbance of the sample was determined at 517 nm. The following equation was used to determine the DPPH scavenging activity:

$$\text{DPPH scavenging activity (\%)} = (\text{abs control} - \text{abs sample}) / \text{Abs control} \times 100$$

where $\text{Abs}_{\text{control}}$ = the absorbance of the control solution (no sample). $\text{Abs}_{\text{sample}}$ = the absorbance of the sample solution.

2.5. Reducing Power Assay

Following the procedure, we measured the reducing power assay at Fe^{3+} to Fe^{2+} transitions in the presence of *A. agallocha* and *A. malaccensis* ethanolic extract [35]. According to this protocol, the aliquot part of different concentrations of the standard (gallic acid) and extracts was mixed with 205 μL phosphate buffer (PH 6.6) and 250 μL of 1% potassium ferricyanide. The mixture was incubated for 20 min at 50 $^\circ\text{C}$. After incubating, 250 μL trichloroacetic acid (10%) was added and centrifuged at 3000 rpm for 10 min. Next, 50 μL supernatant of the solution was mixed with the same amount of distilled water, then 10 μL FeCl_3 (0.1%) was added. Control was prepared without adding extract. The absorbance was measured at 700 nm by using an Elisa reader.

2.6. In Silico Biological Activity Prediction and ADMET Analysis

Based on the chemical structure formula, the biological activity spectrum of substances was predicted using a computational tool called Prediction of Activity Spectra for Substances (PASS) (<http://www.pharmaexpert.ru/passonline/>, accessed on 20 March 2023) [36]. The biological activities of the provided chemicals that are present in the biological system were predicted using this computational technique. This technique also generates a list of pharmacological efficacies together with probabilities for active (Pa) and inactive (Pi) states. Based on precisely calculated predicted probability scores, the accuracy of biological activity was determined; when Pa is close to 1 and Pi close to zero, the chemical is more likely to have biological effects. It is crucial to recognize ADMET traits in order to introduce adverse reactions of a medication candidate at the start of the drug development process. Therefore, we have employed the ADMETlab 2.0 [37] web server to predict the ADME, physicochemical properties, and toxicity properties of Grewin and BDA-366.

2.7. Molecular Docking

The BCL-2 [PDB ID: 4LVT], p53 [PDB ID: 5BUA], BAX [PDB ID: 4S0O], Casp 3 [PDB ID: 5I9B], Casp 9 [PDB ID: 2AR9] protein, and the Protein Data Bank (PDB) were used to obtain the 3D structure [38–42]. For the docking studies, the protein structures were prepared by AutoDock tool graphical interface (GUI) [43]. The receptors also received Kollman charges and polar hydrogen. Fifteen major compounds were selected from *Aquilaria agallocha* Roxb. and *Aquilaria malaccensis* Lam. (Grewin, Aquillochin, Norketoagarofuran, Jinkohol, 10-epi-gamma-eudesmol, Baimuxinal, Gmelofuran, Agarospirol, Agarol, Kusunol,

Beta-Agarofuran, Calarene, Alpha-Agarofuran, Hinesol, and Jinkohol II) according to the previously reported literature study. The Autodock Vina program ran docking simulations using the selected protein structures [44]. The chemicals from BDA-366 served as the study's control. In accordance with our earlier research, precise docking techniques were followed [45,46]. Based on hydrogen bond interactions and binding affinity scores between all of the ligands and proteins, a possible binding interaction was found. To investigate their interactions at the molecular level, the outcomes of each complex were integrated into the DS.3.5 visualizer after being exported from the graphical AutoDock tools interface.

2.8. Molecular Dynamics Simulations

In order to assess the stability of the Grewin and *BCL-2* structures, a molecular dynamics (MD) study was carried out utilizing the Gromacs 4.6 (Groningen Machine for Chemical Simulations) tool [47]. MD simulations were conducted using the *BCL-2* protein (apo form), *BCL-2*-BDA-366 (known inhibitor), and *BCL-2*-Grewin complex structures. The PRODRG2 server was used to construct the Grewin and BDA-366 topology files, while the Gromacs software (pdb2gmx) was used to create the topology files for the *BCL-2* protein [48]. We employed the single-point-charge (SPC) in all simulations [49] water model and the Gromacs96 43a1 [50] force field. In accordance with our earlier research, the complete MD simulation process was used [45,51]. The relevant ions (Na⁺ or Cl⁻) were added to neutralize each system (*BCL-2* protein (apo form), *BCL-2*-BDA-366 (known inhibitor), and *BCL-2*-Grewin), and stages for canonical (NVT ensemble) and isothermal-isobaric (NPT ensemble) equilibration were carried out. Furthermore, each system's production of 10 nanoseconds (ns) was done separately. Every two picoseconds (ps), the findings of the MD simulation were saved for analysis on each complex. The root mean square deviation RMSD, RMSF, and secondary structures were also determined using gromacs functions such as *g_rms*, *g_rmsf*, and *do_dssp*. The docking and molecular dynamics simulations were carried out on an Intel® 2.93 Ghz Xenon® CPU 5670 CentOS server.

2.9. Cell Culture

RAW 264.7 murine macrophage and HaCaT (human keratinocyte) cells were cultured in Dulbecco's Modified Eagle's Medium (DMEM) with 10% fetal bovine serum and 1% penicillin-streptomycin. In a medium comprising 89% RPMI, 10% FBS, and 1% penicillin-streptomycin, human lung carcinoma (A549) was developed. At 37 °C, all cells were kept in a humidified incubator with 5% CO₂ and 95% atmosphere for 24 h.

2.10. In Vitro Cytotoxicity of *Aquilaria agallocha* and *Aquilaria malaccensis*

The cytotoxicity of *A. agallocha* and *A. malaccensis* was examined using an MTT solution in A549, RAW 264.7, and HaCaT cell lines. Then, healthy and cancerous cells were seeded on a 96-well plate at a particular density of 1×10^4 cells every well. After 24 h of stability, cancerous (A549) and normal (RAW 264.7) cells were applied to a range of concentrations (0, 15.625, 31.25, 62.5, 125, 250, 500, 1000) µg/mL, and HaCaT cells were exposed to several concentrations (25, 50, 100, 200, and 400) µg/mL for additional 24 h of incubation. Following a 24 h incubation period, cells were exposed to 20 µL of MTT solution for 3–4 h at 37 °C. Additionally, living cells produce a purple color formazan in response to the presence of MTT solutions. The undissolved formazan agents were dissolved by adding 100 L of DMSO to each. The information was gathered employing a 570 nm ELISA machine from BioTek Instruments, Inc. in Winooski, VT, USA.

2.11. Evaluation of ROS Generation

2',7'-Dichlorodihydrofluorescein diacetate was employed to measure the ROS's activity in A549 and RAW 264.7. We planted the cells in a 96-well cell culture dish at a density of 1×10^4 per well and permitted cells to achieve complete confluency the following day. Cancer cells (A549) were supplemented with various concentrations (0 to 1000) µg/mL for producing ROS generation. On the other hand, RAW 264.7 cells were treated with samples

along with LPS for stimulating the inflammation. Following a 24 h treatment period, the cells were stained in each well with 100 μ L of a DCFH-DA (10 μ M) solution and let sit for 30 min in the dark. After that, the old media was discarded after the cells had been washed twice with PBS (100 μ L/well). A multi-model plate reader (spectrofluorometer) was operated to measure the fluorescence intensity of ROS production with an excitation wavelength of 485 nm and an emission wavelength of 528 nm. The DCFH-DA reagent was utilized to assess the increase in ROS.

2.12. Measurement of Nitrite Levels

In a 96-well plate, RAW 264.7 cells (1×10^4 cells/well) were planted and stabilized for 24 h. Following that, samples of *A. agallocha* and *A. malaccensis* were added to the cells at varying doses for 1 h. Following treatment, the cells were stimulated with *E. coli* lipopolysaccharides (LPS) and maintained for another 24 h. Following the manufacturer's directions, the quantity of nitric oxide (NO) in cultured supernatant media was determined using a Griess reagent. In conclusion, 100 μ L of Griess agent and 100 μ L of stimulated supernatant were mixed up. Using a microplate reader (Bio-Tek Instruments, Inc., Winooski, VT, USA), the resultant absorbance at 540 nm was evaluated in comparison to a standard curve made using sodium nitrite. L-NMMA was utilized as a positive control (standard inhibitor) in this experiment at a dose of 50 μ M. The data were represented as NO production (%) after three runs of each experiment.

2.13. Wound-Healing Assay

To examine the A549 cancer cells' capacity for migration, a wound-healing assay was conducted. In short, 6-well plates containing A549 lung cancer cells were seeded at a quantity of 2×10^4 cells per well, and the plates were then incubated for 1 day at 37 $^{\circ}$ C. Using a 200 μ L sterile pipette tip, the monolayer was scratched vertically, and separated cells were eliminated using PBS. After that, cells were exposed to *A. agallocha* and *A. malaccensis* at doses of 500 and 1000 μ g/mL, and after 3 days of the treatment period, photographs were taken using the implanted 5.0-megapixel MC 170 HD camera (Wetzlar, Germany).

2.14. Gene Expression Analysis

A549 (1×10^4 cells each mL) were plated into a 6-well cell culture dish and maintained for 24 h. The cell culture media was changed and replaced with a fresh medium that contained both samples in varying concentrations for 24 h. Using QIAzol lysis solution (QIAGEN, Germantown, MD, USA), total RNA was extracted after the cells had been rinsed twice with PBS. Following the manufacturer's instructions, the reverse transcription technique was operated using 1 μ g of total RNA from A549 cells in twenty microliters of amfiRivert reverse transcription agents (GenDepot, Barker, TX, USA). The process was run at the following temperatures: for five minutes each at 25 $^{\circ}$ C, sixty minutes each at 42 $^{\circ}$ C, and fifteen minutes each at 70 $^{\circ}$ C. The RT-PCR reaction was carried out thirty-five times for thirty seconds each at 95 $^{\circ}$ C, 60 $^{\circ}$ C, and 72 $^{\circ}$ C. The amplified RT-PCR data were evaluated on 1% agarose gels, stained with DNA Gel Staining, and captured in UV light. Quantitative real-time PCR (qRT-PCR) was carried out in this instance utilizing a SYBR TOPreal qPCR2X Premix from Enzynomics in Daejeon, Republic of Korea. Briefly stated, the reactions were run three times and included 10 μ L of the final solution, 2 \times Master Mix, 1 μ L of template cDNA, and 1 μ L of forward and reverse primers. The aCFX Connect real-time PCR (Bio-Rad, Hercules, CA, USA) was used for all real-time measurements. The following conditions were used to amplify the reactions: 95 $^{\circ}$ C for 10 min, then 40 cycles of 95 $^{\circ}$ C for 20 s, 55–60 $^{\circ}$ C for 30 s, and 72 $^{\circ}$ C for 15 s. The threshold cycle (Ct) for each reaction was estimated using the formula $2^{-\Delta\Delta C_t}$ and the GAPDH gene was utilized to standardize the results. Table S11 primer sequences used in qRT-PCR to analyze the expression of mRNA.

2.15. Measurement of Antioxidant Enzyme Activity

A. A. and A.M extracts were applied to cells in a 6-well plate at a concentration of 50 µg/mL; later, they had been seeded at 1×10^5 cells per well. After 1 day, 500 µM of H₂O₂ was utilized in every well and kept in the incubator for 12 h. The cells were rinsed with PBS twice. The cells were then provided with Triton X-100 (1%) and kept on ice for ten mins. The lysates were kept at $-80\text{ }^\circ\text{C}$ for 1h and centrifuged at 12,000 rpm for 30 min at $4\text{ }^\circ\text{C}$ after defrosting to remove the cellular debris. By utilizing the Bradford protein test (Bio-Rad, Hercules, CA, USA), the entire protein content was calculated.

2.16. Measurement of SOD Activity

As previously described but with changes, SOD activity was assessed [27]. Briefly, 50 µg of protein, 50 mM phosphate buffer (pH = 10.2), and 10 mM epinephrine were added to a 96-well plate. The kinetics of absorbance of the pink-colored product was measured at 490 nm for 10 min using a microplate reader. In units/mg protein, the quantity of enzyme necessary to trigger a 50% inhibition of epinephrine autoxidation was calculated.

2.17. Measurement of GPx Activity

In order to monitor GPx activity, we used the approach previously described by [52], with some modifications. Briefly, 50 µg of protein was added to a reaction mixture of 100 mM phosphate buffer (pH = 7), 1 mM EDTA, 1 mM NaN₃, 10 mM GSH reduced, 1 unit of glutathione reductase, and 1.5 mM NADPH. For five minutes, the absorbance at 340 nm was observed. A change in absorbance at 340 nm was used to determine GPx activity as the rate of NADPH oxidation. The units/mg protein represent the amount of enzyme needed to oxidize 1 mM NADPH.

2.18. Measurement of CAT Activity

CAT activity was measured as previously described, with modifications [27]. Briefly, 50 µg of protein and 100 mM phosphate buffer (pH = 7), and 100 mM H₂O₂ were added to a 96-well plate, and the reaction mixture was incubated for 2 min at $370\text{ }^\circ\text{C}$. A microplate reader was used to measure the absorbance at 240 nm for 5 min. According to the H₂O₂ oxidation process, the absorbance changed with time. Units/mg protein were used to express the volume of the enzyme needed to degrade 1 mM of H₂O₂.

2.19. Measurement of GST Activity

GST activity was measured as previously described by [53] with modifications. The assay was carried out in 100 mM phosphate buffer (pH = 7.5) containing 1 mM CDNB and 1 mM GSH reduced. The change in absorbance upon conjugation of glutathione and CDNB were measured in a microplate reader at 340 nm for 10 min.

3. Results and Discussion

3.1. TPC, TFC, and Antioxidant Activities

It is well-recognized that free radicals contribute significantly to a broad range of clinical symptoms. Antioxidants combat free radicals and shield us from illness. They either remove reactive oxygen species from the environment or defend the antioxidant defense system [54]. In our current observation, *A. malaccensis* contains substantially more flavonoids and phenolic compounds than *A. agallocha*. Additionally, flavonoids have properties that help to stop cell damage [55]. During normal growth, phenolic compounds are also secondary metabolites produced in plants and play an essential role in wound treatment and skin infection [56]. During normal growth, phenolic compounds are also secondary metabolites produced in plants and play a vital role in wound treatment and skin infection [57]. The extract of *A. agallocha* is a considerably higher phenolic compound than others.

TPC and TFC were determined by the Folin–Ciocalteu (FC) and aluminum chloride colorimetric methods. Table 1 revealed the TPC and TFC of *A. Agallocha* and *A. malaccensis*

extracts where gallic acid and rutin were used as standard, respectively. TPC values of *A. agallocha* and *A. malaccensis* were 37.203 ± 0.14 and 30.026 ± 0.11 $\mu\text{g GAE/mg}$, whereas total flavonoid contents were 276.745 ± 0.09 and 292.095 ± 0.08 $\mu\text{g RE/mg}$, respectively.

Table 1. Total phenolic and flavonoid content of ethanolic extracts of *A. agallocha* and *A. malaccensis*.

Samples	Total Phenolic Contents ($\mu\text{g GAE/mg Extract}$)	Total Flavonoid Contents ($\mu\text{g RE/mg Extract}$)	In Vitro Antioxidant	
			DPPH Scavenging ($\mu\text{g/GAE mg Extract}$)	Reducing Power ($\mu\text{g/GAE mg Extract}$)
<i>A. agallocha</i>	37.203 ± 0.14	276.745 ± 0.09	2.394 ± 0.009	9.746 ± 0.06
<i>A. malaccensis</i>	30.026 ± 0.11	292.095 ± 0.08	2.271 ± 0.006	9.243 ± 0.03

According to the DPPH assay, *A. agallocha* showed better antioxidant activity than *A. malaccensis*. We noticed that *A. agallocha* exhibited 2.394 ± 0.009 $\mu\text{g/GAE mg extract}$, whereas *A. malaccensis* showed 2.271 ± 0.006 $\mu\text{g/GAE mg extract}$. In addition, the reducing power assay assessed the reducing ability of *A. agallocha* and *A. malaccensis* extracts in a redox reaction. The results of the reducing power assay were revealed as gallic acid equivalent and *A. agallocha* and *A. malaccensis* extracts exhibited 9.746 ± 0.06 and 9.243 ± 0.03 $\mu\text{g GAE equivalent}$, respectively.

3.1.1. Biological Activity Prediction and ADMET Analysis

Using the PASS software, which predicts the biological reaction spectra according to the atomic structure equation, significant biological targets for Grewin have been found. This application was used to determine the targets from the original chemical structure using the multilevel neighborhoods of atoms (MNA) descriptor. The Pa and Pi scores are between 0 and 1, and can be predicted using these MNA descriptors. Depending on Pa values near 1 and Pi values close to 0, it is possible to identify the biological target active molecules [58]. The results of Grewin indicated that the following targets may have biological activity: TP53 expression enhancer, hepato-protectant, monophenol monooxygenase inhibitor, free radical scavenger, membrane integrity agonist, antimutagenic, caspase 3 stimulant, anticarcinogenic, UDP-glucuronosyltransferase substrate, chemo-preventive.

Table 2 displays the predicted objectives for Grewin as well as the Pa and Pi values. The predicted values of the other four highly ranked compounds according to the docking studies are given in (Tables S1–S4).

Table 2. Grewin's predicted biological activity.

Predicted Biological Activity	Pi ^a (%)	Pa ^b (%)
TP53 expression enhancer	0.907	0.002
Hepato-protectant	0.907	0.002
Monophenol monooxygenase inhibitor	0.907	0.002
Free radical scavenger	0.906	0.002
Membrane integrity agonist	0.850	0.024
Antimutagenic	0.816	0.004
Caspase 3 stimulant	0.811	0.005
Anticarcinogenic	0.803	0.005
UDP-glucuronosyltransferase substrate	0.794	0.007
Chemo-preventive	0.741	0.005

^a Pa denotes the probability of active. ^b Pi symbolizes the probability of inactive.

This study analyzed the ADME of Grewin and the control drug BDA-36 using the ADMETlab 2.0 [37]. This analysis represents chemical compounds' physicochemical properties and their biological functions. These physical, chemical, and biological characteristics

are the following parameters were calculated: number of atoms, molecular weight, formal charge, number of rigid bonds, number of heteroatoms, number of rotatable bonds, topological polar surface area, number of hydrogen bond donors, number of hydrogen bond acceptor, logP at physiological pH 7.4, log of the aqueous solubility, and log of the octanol/water partition coefficient (Figure 1). For oral absorption, molecules with a molecular weight (MW) of 500 Da or less are preferred; molecules with a greater MW are absorbed across the membrane. Therefore, Grewin passes Lipinski's rule of five and Pfizer rule. Human intestinal absorption (HIA), human oral bioavailability F20% and F30%, human colon adenocarcinoma cell lines (Caco-2) permeability, Madin-Darby canine kidney cells (MDCK) permeability, P-glycoprotein inhibitor (Pgp-inhibitor), and Pgp-substrate were computed to assess the absorption of Grewin. Grewin showed good Caco-2 and MDCK permeability. It is also an excellent Pgp inhibitor showing good oral bioavailability. All of the compounds' other physicochemical characteristics were found to be acceptable and superior to those of the control medications, qualifying them as lead molecules. (Tables S5–S10).

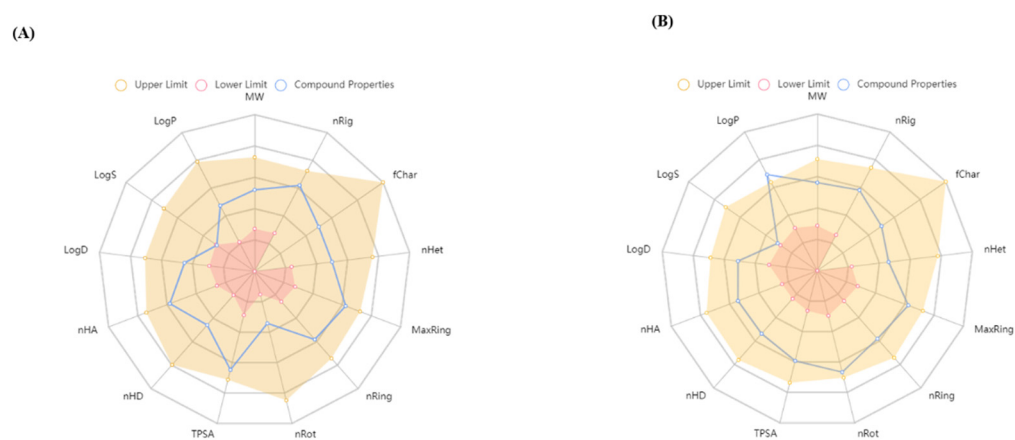


Figure 1. ADMET properties of (A) Grewin; (B) BDA-366. Abbreviations: MW: Molecular weight; nRig: number of rigid bonds; fChar: formal charge; nHet: number of heteroatoms; MaxRing: number of atoms in the biggest ring; nRing: number of rings; nRot: number of rotatable bonds; TPSA: topological polar surface area; nHD: number of hydrogen bond donors; nHA: number of hydrogen bond acceptor; LogD: logP at physiological pH 7.4; logS: log of the aqueous solubility; and LogP: log of the octanol/water partition coefficient.

3.1.2. Molecular Docking Interaction

The molecular level interaction of *BCL-2*, *Bax*, *p53*, *Casp 3*, and *Casp 9* protein and the 15 compounds from *Aquilaria agallocha* Roxb. and *Aquilaria malaccensis* Lam. was analyzed using the molecular docking method. This work used the AutoDock Vina program to run a docking simulation using the crystal structures of the proteins *BCL-2*, *Bax*, *p53*, *Casp 3*, and *Casp 9*. The known inhibitor BDA-366 was utilized as a control, and the crucial active site residues were kept flexible. The creation of hydrogen bonds and the binding energy to the important active residues and the chosen compounds served as confirmation of the interaction results. According to the analysis of docking results, Grewin interacts with *BCL-2* via two hydrogen bonds (ASP108 and ARG143) with binding affinities of -7.5 kcal/mol each. The control drug BDA-366 and Grewin establish two hydrogen bonds, one of which is similar to that of the control drug. The detailed docking results of the best compound with *BCL-2* and the control ligand are shown in Table 3. An illustration showing the interactions of Grewin and BDA-366 with the residues in the active site of *BCL-2* Figure 2A,B. The 2D interaction diagram for the top five ligands with each of the proteins employed in this investigation is also included in Supplementary Materials Tables S1–S11. Surprisingly, among all the 15 compounds from this study, Grewin ranked best among all the proteins used. These results showed that Grewin is a promising compound in treating cancer and inflammation. It also further reveals that the presence of Grewin and the fifteen other compounds in the extracts of *Aquilaria agallocha* Roxb. and *Aquilaria malaccensis* Lam.

might be the reason for its anti-cancer and anti-inflammatory activity, which needs further evaluation. The docked ligands Grewin and BDA-366 with *BCL-2* were further subjected to MD simulation.

Table 3. Interaction of compounds from *Agallocha* with amino acid residue of *BCL-2*.

Protein	Compound	Binding Energy (kcal/mol)	Hydrogen Bond Interactions	Hydrophobic Interactions	No. of Hydrogen Bonds
BCL-2	Grewin	−7.5	ASP108; ARG143	PHE109; MET112; ALA146	2
	Gmelofuran	−7.4	-	ARG104; LEU198; PHE195	0
	BDA-366	−6.3	LEU134; ARG143	ALA146; GLU133; TRY105	3

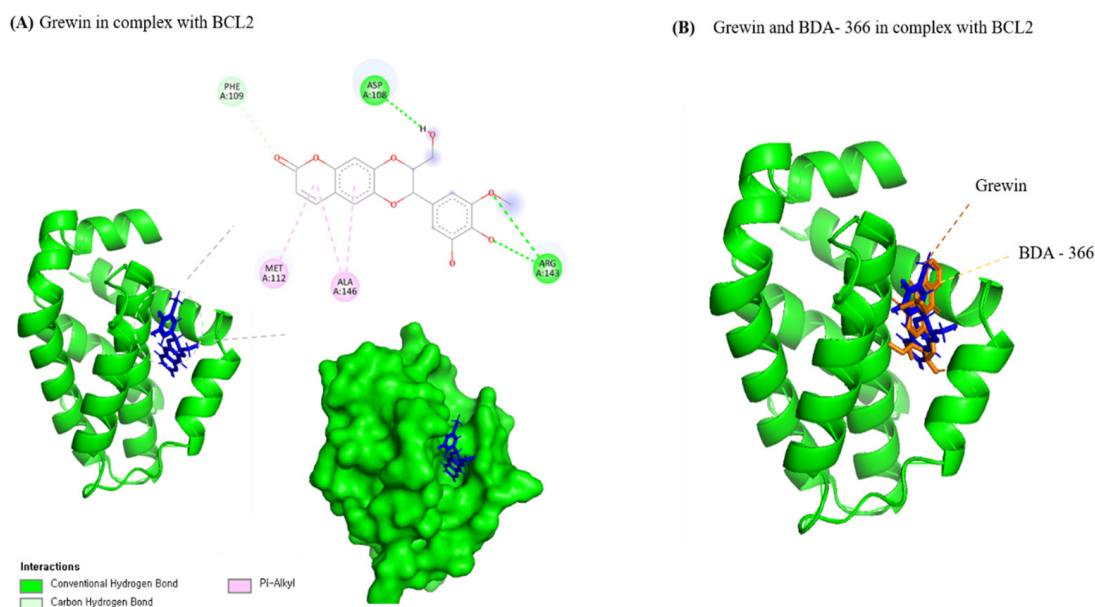


Figure 2. (A) Two-dimensional and three-dimensional docking interactions of Grewin with *BCL-2*. (B) Grewin and BDA-366 in complex with *BCL-2* (Blue—Grewin, Orange—BDA-366).

3.1.3. Analysis of Molecular Dynamics

The molecular dynamics (MD) approach was used to apply structural evolution to the docked complex structures of *BCL-2* interaction. This work ran three separate MD simulations on the apo form of *BCL-2*, the complexes of *BCL-2* with the known inhibitor BDA-366, and *BCL-2* with Grewin. The examination of MD data is displayed in Figures 3 and 4. The RMSD versus the skeleton of every complex (after each complex had reached equilibrium, stability persisted for the whole 10 ns simulation period). In addition, throughout the simulation versus C atoms, root means square fluctuation (RMSF) analysis of all the complexes was computed. The computed RMSF values for each complex are shown in Figure 3B. After that, the compactness of the protein–ligand complexes analyzed by recording the ROG values were also obtained. For every complex, the radius of gyration is determined, as shown in Figure 4A. Further, Figure 4B shows the number of hydrogen bonds that have been computed and calculated. According to an MD simulation research, Grewin can effectively interact with *BCL-2* to create a stable complex that is comparable to the control medication BDA-366.

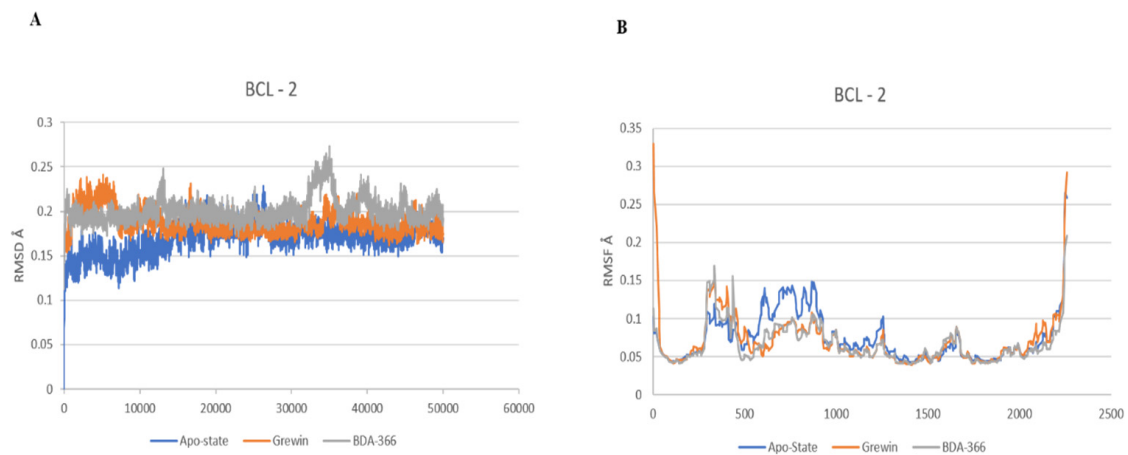


Figure 3. (A) RMSD of Grewin and control (BDA-366) in complex with BCL-2. (B) RMSF of Grewin and control (BDA-366) in complex with BCL-2 as a function of MD simulation time.

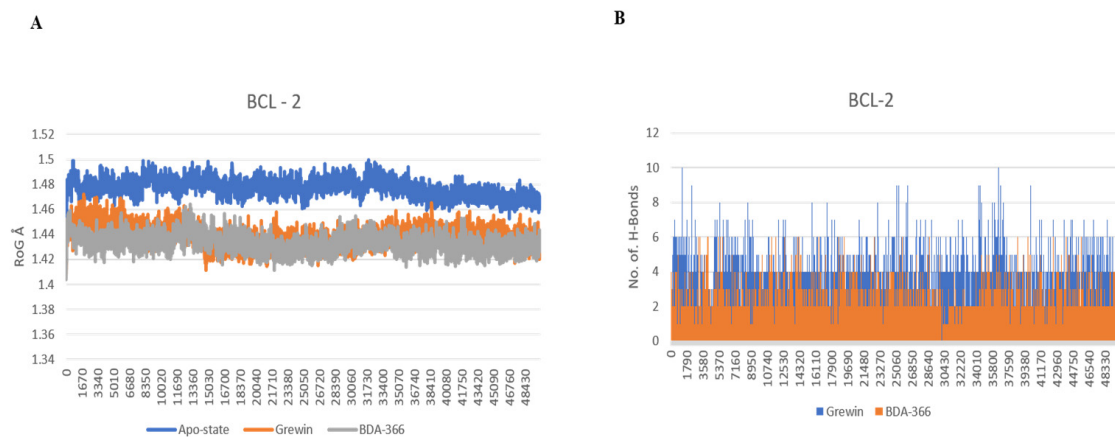


Figure 4. (A) Radius of gyration plots of molecular dynamics (MD) simulation of BCL-2 Grewin and control (BDA-366) complexes. (B) Line plots of ligand–protein H bonds for BCL-2 with Grewin and control (BDA-366).

3.2. Evaluation of Cytotoxicity

For the development of medications to treat different diseases, natural bioactive compounds are a promising source. Particularly, it has been demonstrated that a number of natural plants have pharmacological benefits, such as anti-inflammatory, anti-cancer, and antioxidant capabilities [59–61]. To examine the toxicity of the samples, *A. agallocha* and *A. malaccensis* were subjected to cytotoxic evaluation against RAW 264.7 cells and A549 cancer cells (Figure 5). In the cytotoxicity experiment, we measured the level of cell toxicity using an MTT solution. It was discovered that when exposed to A.A. and A.M at 15.625 to 1000 $\mu\text{g}/\text{mL}$ for 24 h, RAW 264.7 cells displayed low levels of toxicity and high cell viability. However, as compared to the control, 1000 $\mu\text{g}/\text{mL}$ of *A. agallocha* and *A. malaccensis* suppressed cell proliferation by 50–55% in the A549 cells. Contrarily, the viability of A549 cells was discovered to be diminished by *A. agallocha* and *A. malaccensis* in a dose-dependent way. HacaT cells were added to both samples at different doses for 24 h, ranging from 25 to 400 $\mu\text{g}/\text{mL}$, for the purpose of antioxidant enzyme tests. At 50 $\mu\text{g}/\text{mL}$, both samples showed less toxicity on the normal cell. We concluded that both samples were considered to be safe for non-cancerous cells and significantly toxic for cancer cells.

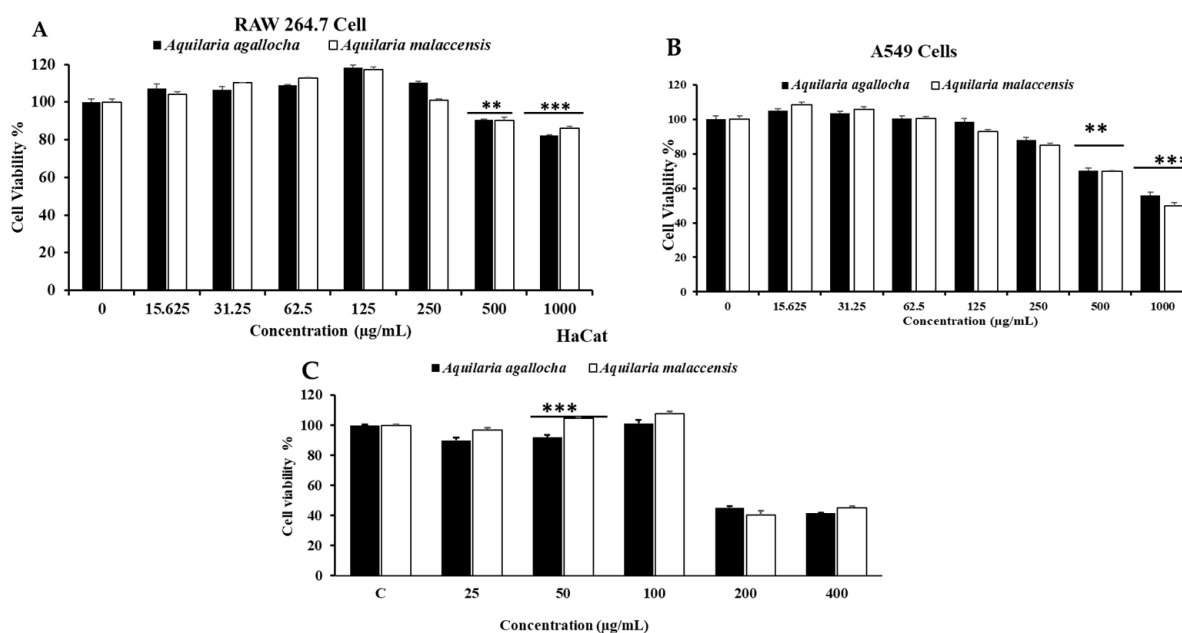


Figure 5. An assessment of the cytotoxicity of *A. agallocha* and *A. malaccensis* to cells (A) on (RAW 264.7), (B) on lung carcinoma (A549) cells, (C) HaCaT cell lines compared to non-treated cells. The graph displays the means and standard deviations for the four replicates. Significant differences from control sets are mentioned by ** $p < 0.01$; and *** $p < 0.001$.

3.2.1. In Vitro ROS Induced by *A. agallocha* and *A. malaccensis* on Cancer Cells

Reactive oxygen species (ROS) are essential for producing cytotoxicity in cancer cells higher levels of ROS buildup have been found to trigger apoptosis, cell cycle arrest, and autophagy, in a number of human cancer cell lines [62–64]. Reactive oxygen species (ROS) contribute to cellular signaling and are produced naturally as byproducts of regular cell activity [65]. Because of a mismatch among oxidizing substances and antioxidants, cancer cells usually have baseline ROS levels that are higher than those of normal cells. ROS at low levels serve as second messengers inside cells. Because they can enhance cancer metabolism and growth signals and suppress antioxidants, which promote oncogenesis, moderate levels of ROS are advantageous to cancer cells. In contrast, high ROS concentrations may lead to DNA damage-related cell death [66–68]. Due to the production of reactive oxygen species (ROS), *A. agallocha* and *A. malaccensis* are essential reputable materials for anti-cancer action [69]. The DCFH-DA reagent was added in this instance to determine the intracellular ROS level in both samples on A549 cells. In comparison to the control, a dose-dependent increase in internal ROS production was seen in the malignant A549 cells after treatment with *A. agallocha* and *A. malaccensis* at higher concentrations (1000 µg/mL) (Figure 6). Research findings have revealed that an elevate in ROS formation and apoptosis are correlated with a decrease in mitochondrial membrane potential. Reactive oxygen species (ROS) are created by mitochondria during apoptosis [70,71]. The buildup of ROS may also trigger the development of p53, which has a substantial impact on the beginning of apoptosis by activating pro-apoptotic proteins (*Bax*) or inhibiting anti-apoptotic mitochondrial proteins (*BCL-2*) [31,72]. *A. agallocha* and *A. malaccensis* extracts inhibited cell growth and produced ROS, which suggests that ROS generation promotes apoptosis via the mitochondrial pathway in A549 lung cancer cells.

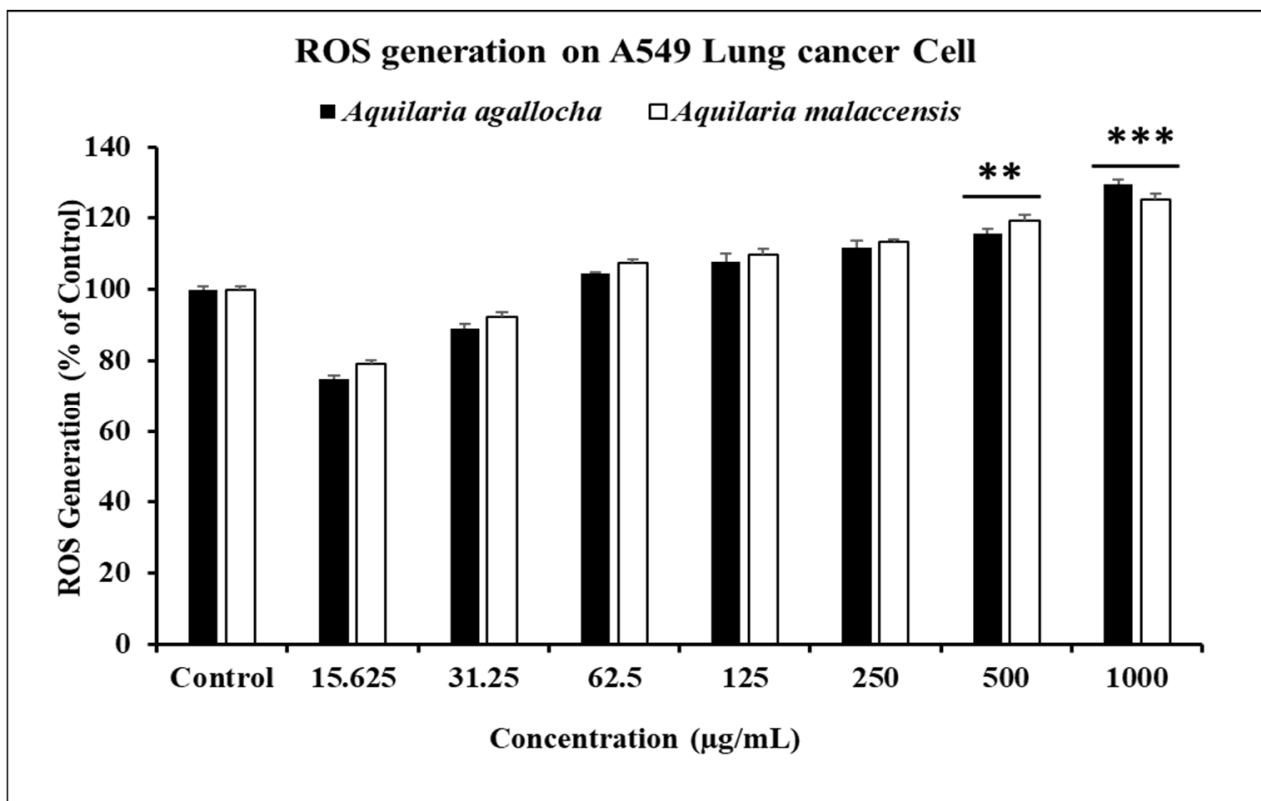


Figure 6. The capacity of *A. agallocha* and *A. malaccensis* to produce intercellular ROS in A549 cells was compared to control. The graph displays the mean and standard deviation for the three replicates. Significant deviations from control groups are denoted by ** $p < 0.05$; *** $p < 0.001$.

3.2.2. *A. agallocha* and *A. malaccensis* Extract Increased NO Production and Inhibited ROS Generation Induced by LPS

Appropriate NO production in mammalian cells is important for many basic physiological processes [73,74]. However, excessive NO production can result in a number of chronic and acute illnesses, including inflammation, cancer, and sepsis. One of the most significant pro-inflammatory mediators is nitric oxide (NO). Inhibiting the overproduction of nitric oxide levels is thus a desirable target in the search for new anti-inflammatory drugs. We examined the anti-inflammatory properties of the chosen *A. agallocha* and *A. malaccensis* on the reduction of NO generation in LPS-stimulated RAW 264.7 cells at concentrations of (15.625 to 1000 µg/mL). At 1000 µg/mL concentration, both samples showed strong significant reductions in LPS-induced NO production (44.73% and 46.91%, respectively), in a dose-dependent way, whereas L-NMMA was employed in this investigation as a positive control for inhibiting NO production. On the other hand, as a result of the immune response's increased ROS production during inflammation and the body's altered oxidant/antioxidant balance, DNA, proteins, and lipids are damaged [75]. RAW 264.7 cells were subjected to various meditations of *A. Agallocha* and *A. malaccensis* in the presence or absence of LPS for 24 h to examine the inhibitory effects of both species on LPS-induced ROS generation. As shown in Figure 7, ROS production was more elevated in the LPS-treated group than in the control and only LPS-treated group.

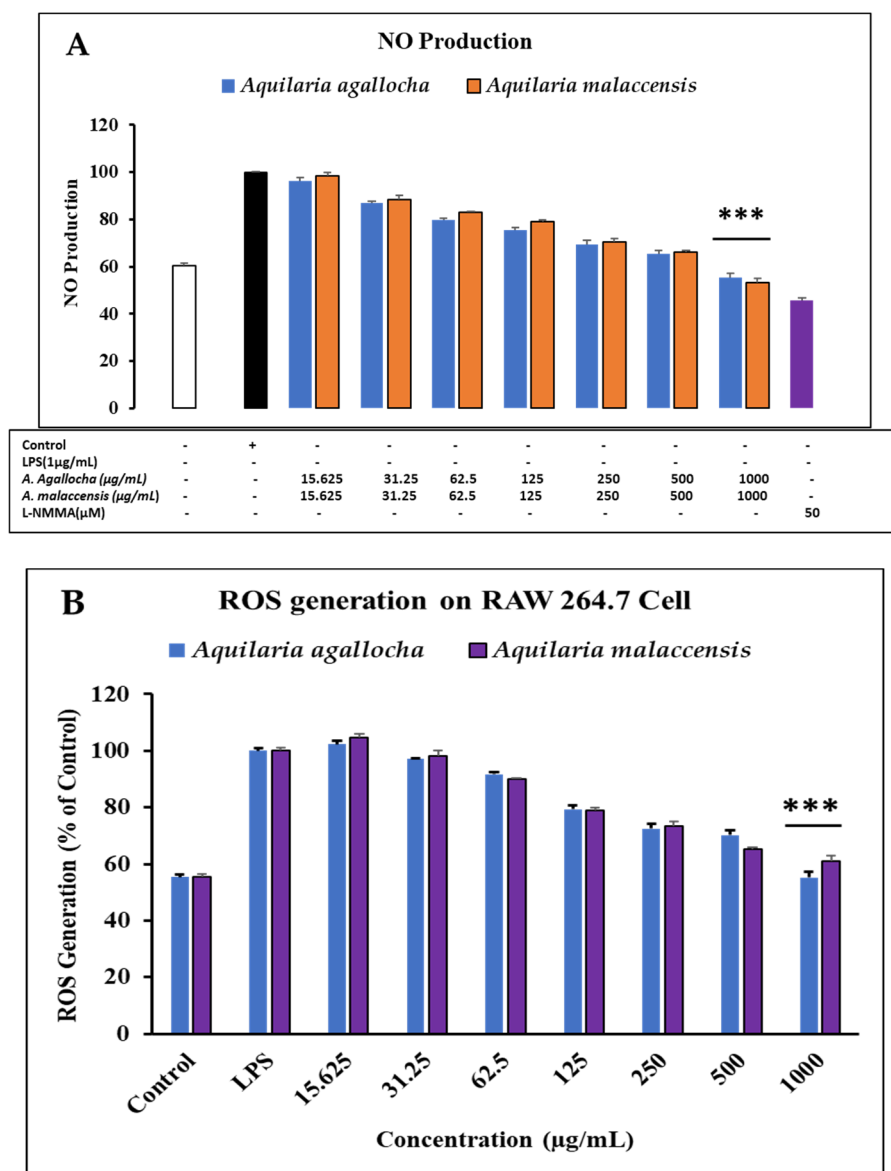


Figure 7. The effects of *A. agallocha* and *A. malaccensis* on (A) NO generation were assessed using RAW 264.7 cells activated with 1 µg/mL of LPS. (B) Reactive oxygen species (ROS) production within cells was contrasted with control. Data presented as ±SEM, *** $p < 0.01$ vs. control cell. All medication was conducted in triplicate.

3.2.3. Cancer Cells Migration Is Inhibited by *A. agallocha* and *A. malaccensis*

Preventing cancer metastasis is a key objective of cancer treatment because it accounts for 90% of all cancer-related deaths [53]. The hallmarks of a cancer cell’s ability to spread to other tissues are cell invasion and migration. The initial stage in the progression of metastatic malignancies is the invasion of malignant cells into the surrounding tissue and the vasculature [76]. To prevent and cure metastatic cancer, it would be difficult to find targets that block cancer cells from migrating and invading other tissues. A scratch migration assessment was used to inspect the impacts of A.A and A.M on the migration of A549 cells. A wound closure test was used to compare cell migration (%) before and after the treatment of A549 lung cancer cells with A.A and A.M (500 and 1000 µg/mL) (Figure 8). Cells treated with A.A and A.M showed inhibited migration after 24 h. These studies propose that A.A and A.M can stop cancer cells from migrating and metastasizing. In the control group after 24 h, migratory cells had almost filled in all gaps between cell layers. Additionally, cancer cells treated with A.A. and A.M showed an enhanced ability to

prevent migration in contrast to the control group. The ability of A.A and A.M to inhibit growth could suggest that it has potential as an anti-lung cancer treatment.

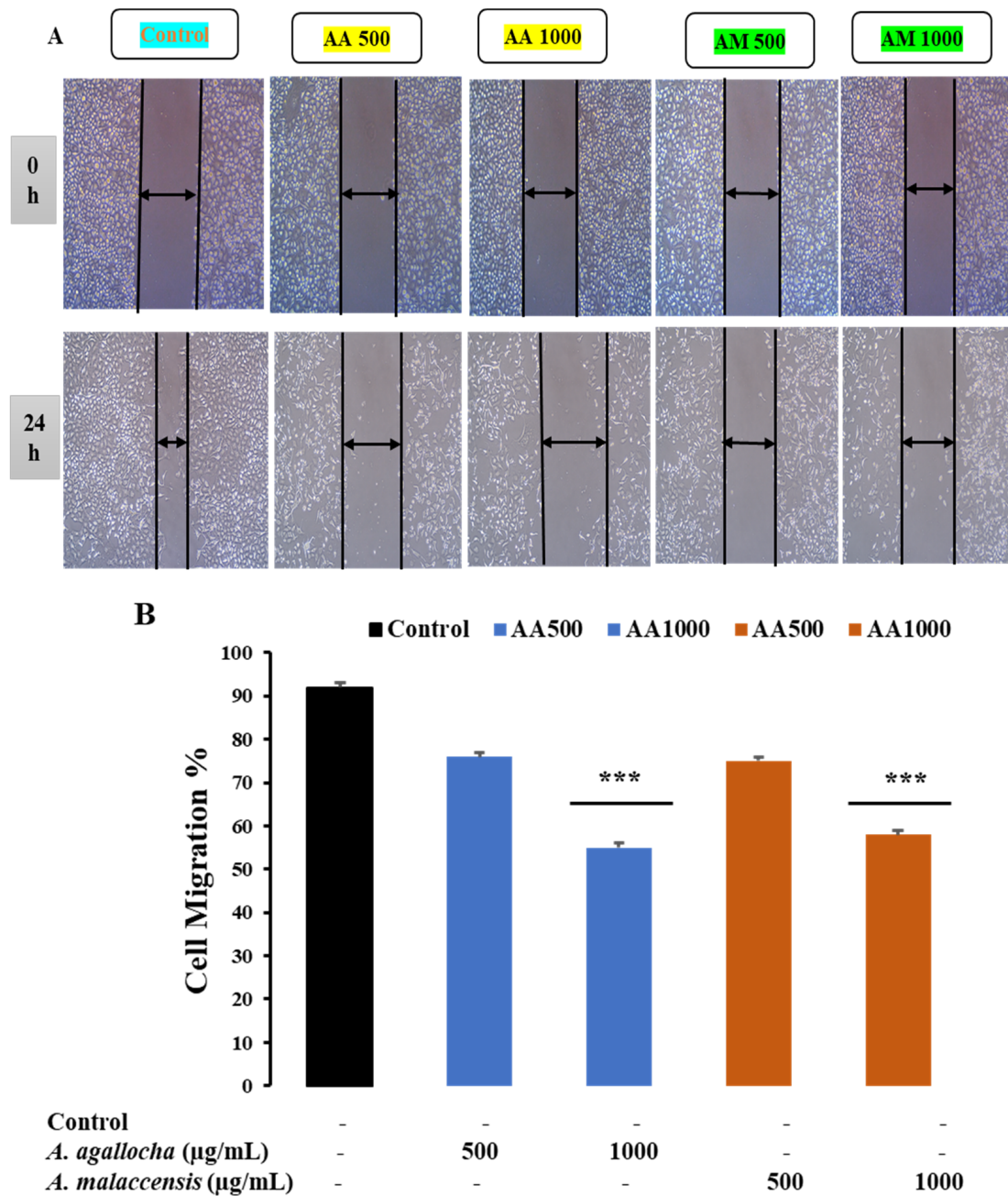


Figure 8. (A) ImageJ software was used to measure the scratched region’s cell-free area. The proportion of scratch cell migration seen 24 h after treatment compared to control data represents the amount of cell migration. (B) Untreated cells are indicated by controls. Values are revealed as mean ± standard deviation, and statistical significance is indicated by *** $p < 0.01$. The scale bar indicates 10× magnification.

3.2.4. By Controlling Apoptotic Gene Expression, *A. agallocha* and *A. malaccensis*-Induced Apoptosis

Redox signaling requires the production of ROS by mitochondria, while the redox-active transcription factor p53 inhibits cancer [77,78]. Numerous pro- and anti-apoptotic genes involving *Bax* and *BCL-2* are regulated by P53. One of the apoptotic pathways, *BCL-2*, is stimulated in response to stressful circumstances, such as DNA damage or cytokine

shortage [79]. This mechanism might have been triggered by mitochondrial-mediated apoptosis, as shown by the downregulation of BCL-2, the overexpression of the caspase 9/3 gene, a rise in *Bax* level, cyto C relief into the cytoplasm, and BCL-2 inhibition [80]. Additionally, *A. agallocha* and *A. malaccensis* significantly upregulated the mRNA expression of the genes *p53*, *Bax*, *Casp 9*, and *Casp 3*, and downregulated the expression of the gene BCL-2 when compared to the control in the RT-PCR (Figure 9). In contrast, *A. agallocha* elevated the mRNA expression of *p53* (1.44 fold), *Bax* (1.91 fold), caspase 3 (1.92 fold) and caspase 9 (1.56 fold), whereas BCL-2 (0.96 fold) downregulate the expression. *A. malaccensis* showed *p53*, *Bax*, BCL-2, *Casp 3*, and *Casp 9* gene expression by (1.56, 1.91, 0.81, 1.72, 1.44) fold, respectively, compared to untreated cells. As a result, this research demonstrated that *A. agallocha* and *A. malaccensis* were able to suppress the expression of the apoptosis gene in lung cancer cells. Therefore, to completely comprehend the biological pathways, Western blot analysis and additional studies (*in vivo* and clinical trials) regarding molecular signaling processes are required.

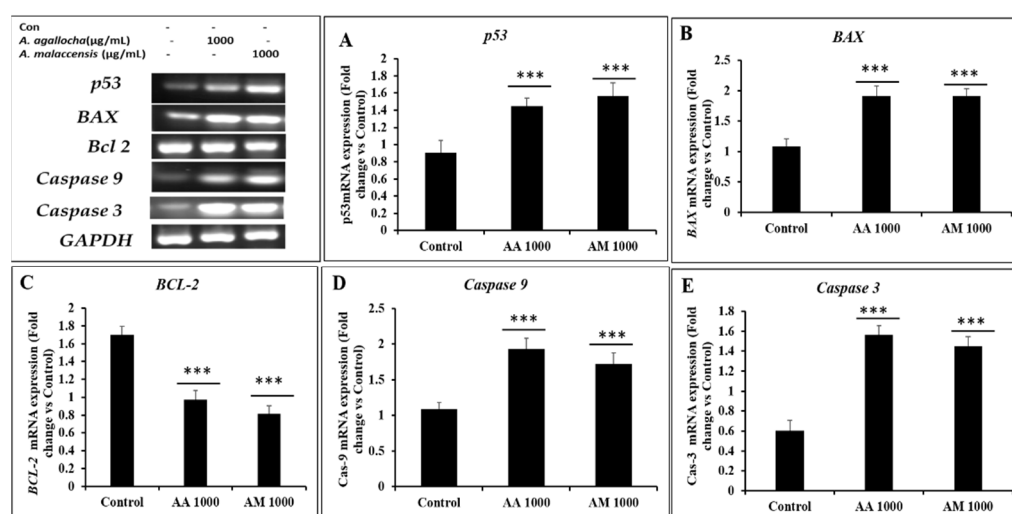


Figure 9. Effects of A.A and A.M on the apoptosis-related genes' levels of mRNA expression in A549 cells. A.A and A.M were applied to A549 cells at a dose of 1000 $\mu\text{g}/\text{mL}$ for 24 h. Following the extraction of total RNA, qPCR was used to analyze the transcript expression levels using primers that targeted (A) *p53*, (B) *Bax*, (C) *BCL-2*, (D) *Caspase 9*, and (E) *Caspase 3*. Every bar displays the mean and standard deviation of both samples from all three separate trials (** $p < 0.01$ utilizing Student's *t*-test contrasted against the control).

3.2.5. *A. agallocha* and *A. malaccensis* Extract Inhibited the Increased Levels of Inflammation-Related Cytokines

An important role for proinflammatory mediators in the development of inflammatory diseases [81]. Asthma, arthritis, and cancer are examples of chronic inflammatory illnesses where these factors, such as *iNOS*, *TNF- α* , *Cox-2*, *IL-1 β* , and *IL-6*, are overexpressed by macrophages [82]. Important inflammatory response signaling pathways including *NF- κ B* and *MAPKs* regulate a range of innate and adaptive immune responses. Both *NF- κ B* and *MAPKs* signaling serve as key regulators of the production of pro-inflammatory mediators during the inflammatory response. Nuclear transcription factors including *MAPKs* and *NF- κ B* can be activated by LPS, stimulating signaling pathways in macrophage cells. Inducible *iNOS*, *TNF- α* , *IL-6*, *COX-2*, and other proinflammatory mediators can all be initiated by macrophage cells when LPS is expressed [83]. Therefore, this study focused on exploring the *A. agallocha* and *A. malaccensis* affected gene expression on those factors by RT-PCR and qRT-PCR. In the LPS-treated group, there was a substantial increase in the mRNA expression of *COX-2*, *TNF- α* , *iNOS*, *IL-6*, and *IL-8*. However, the *A. agallocha* and *A. malaccensis* extracts reduced the gene expression in a dose-dependent way. The *A. agallocha*-treated cell significantly suppressed the gene expression of *COX-2*, *TNF- α* , *iNOS*, *IL-6*, and

IL-8 (1.56, 0.98, 1.91, 1.93, 1.52) fold, respectively. In contrast, *A. malaccensis* treated cells that significantly suppressed the gene expression of *COX-2* (1.44 fold), *TNF- α* (0.81 fold), *iNOS* (1.79 fold), *IL-6* (1.53 fold), and *IL-8* (1.39 fold), respectively (Figure 10). The quantities analysis showed that *A. malaccensis* has more anti-inflammatory activity than *A. agallocha*.

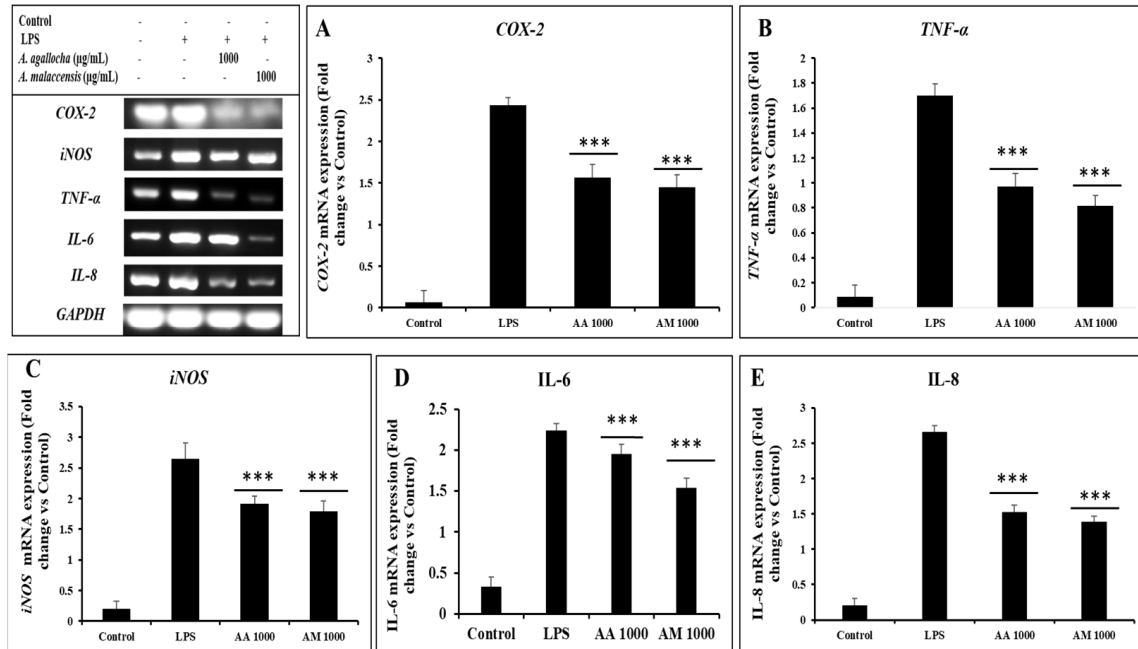


Figure 10. Effects of A.A and A.M on pro-inflammatory mediators (A) *COX-2*, (B) *TNF- α* , (C) *iNOS*, (D) *IL-6*, (E) *IL-8* in LPS induced RAW 264.7 cells. The mRNA expression was determined by qPCR analysis. Data presented as \pm SEM, *** $p < 0.01$ vs. normal. All treatment was observed three times.

3.3. Antioxidant Enzymatic Activity

ROS, which result in oxidative damage to skin cells, are a significant factor in the aging process. The skin is particularly vulnerable to these processes because there are so many possible cellular targets for oxidative injuries. A crucial defense against oxidative cell damage is the antioxidant mechanism [27]. *SOD*, *CAT*, *GPx*, *GST*, and other intrinsic and extrinsic antioxidant enzymes and nutrients make up the antioxidant system, which reduces the toxicity of free radicals [28]. *SOD* slows down the aging process by removing the superoxide anion, which are created in the initial stages of oxidative injury [84]. Superoxide is converted by *CAT* to hydrogen peroxide and oxygen. The fast breakdown of hydrogen peroxide is typically catalyzed by cells using *CAT* and *GPx*. *GSTs* primarily operate as cytoprotectors by activating the conjugation reaction of reduced glutathione (*GSH*), which results in the production of reactive electrophiles. HaCaT cells were medicated with both A.A and A.M, and antioxidant enzyme functions such as *SOD*, *GPx*, *CAT*, and *GST* were assessed to determine whether the antioxidant effects of A.A and A.M are connected to the induction of antioxidant enzyme activity. As displayed in Figure 11, the activities of the 4 enzymes were downregulated by H_2O_2 (100 μ M) treatment during treatment with A.A and A.M. restored the activities of the enzymes more than the control. Through promoting the activity of endogenous antioxidant enzymes, A.A and A.M seem to have antioxidant capabilities.

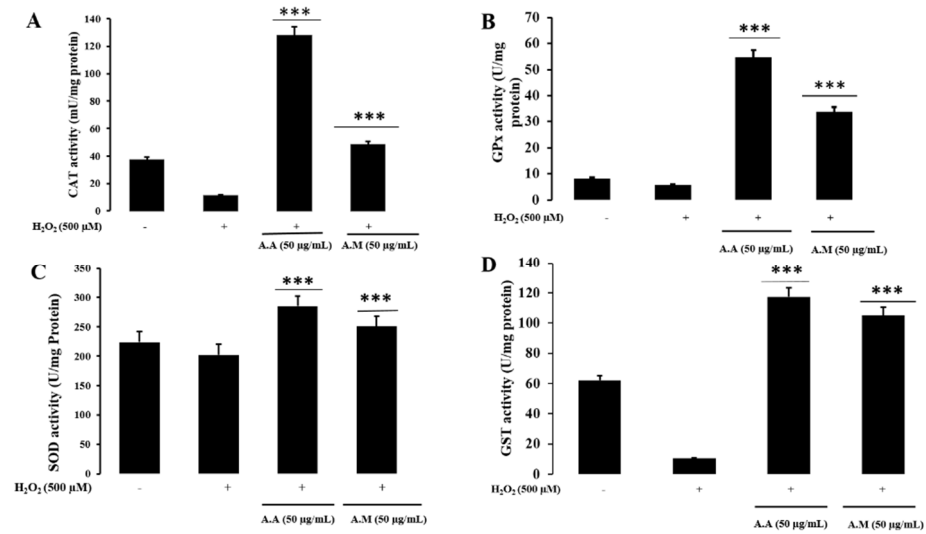


Figure 11. *In vitro*, antioxidant enzymatic activity for *A. agallocha* and *A. malaccensis* (A) CAT (B) GPx (C) SOD (D) GST on Hacat cells compared to non-treated control. Graph shows mean ± SD values of four replicates. *** $p < 0.001$ shows considerable variations from control groups.

Enhancing Antioxidative Gene Expression on Hacat Cells

The RT-PCR presented the upregulation of antioxidant genes such as *SOD*, *CAT*, *GPx*, and *GST* expression in a dose-dependent method via A.A and A.M extracts. Figure 12 shows that pretreatment with plant extracts and ascorbic acid has significantly increased the gene expression levels in the presence of H₂O₂. These outcomes showed that A.A and A.M extract effectively suppress oxidative stress by enhancing antioxidative gene expression in H₂O₂-induced Hacat cells.

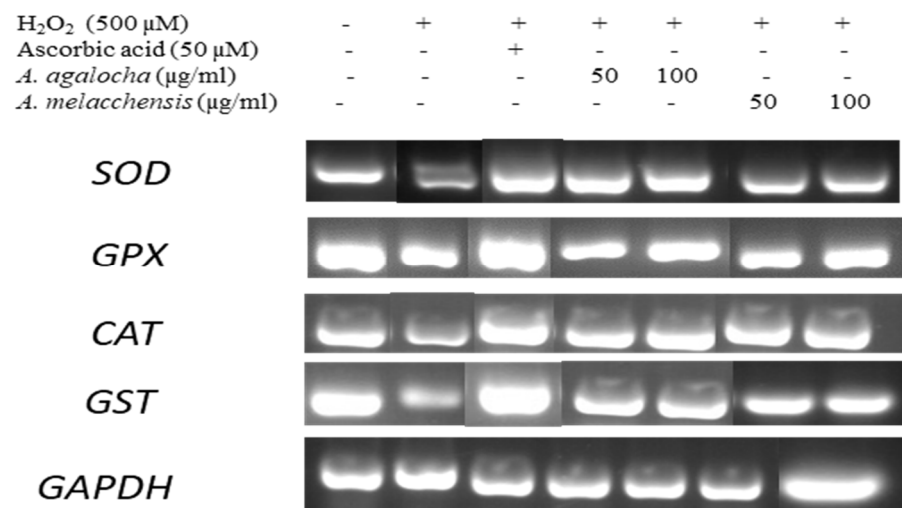


Figure 12. Effects of *A. agallocha* and *A. malaccensis* on mRNA expression levels of antioxidant related genes *SOD*, *GPx*, *CAT* and *GST* in Hacat cells. Compared with positive control (H₂O₂).

4. Conclusions and Future Perspective

Medicinal plants have been utilized as traditional therapies for several human diseases for thousands of years. In this study, we investigated *A. agallocha* and *A. malaccensis* as possible bioactive substances from natural sources for different pharmacological efficacy for anti-cancer, anti-inflammatory, and antioxidant with *in silico* and *in vitro* experiments. Additionally, the *in silico* study revealed that the major constituents of both plants have a significant binding affinity to the sites of the target proteins (*BCL-2*, *Bax*, *p53*, *Casp 3*, and *Casp 9*). Among them, Grewin has shown stable and favorable energies, causing strong

binding with the target. Accordingly, the *in vitro* study also observed that A.A and A.M are less toxic on RAW cells inhibiting NO production and intercellular ROS generation and suppressing the pro-inflammatory mediators such as (COX-2, TNF- α , iNOS, IL-6, and IL-8). On the other hand, A.A and A.M extract effectively suppress oxidative stress by enhancing antioxidative gene expression (SOD, CAT, GPx, GST) in H₂O₂-induced Hacat cells. Interestingly, anti-cancer results revealed significant toxicity on cancer cells with upregulating of ROS levels that inhibited cell migration and apoptosis in cancerous cells. Accordingly, both plant extracts increased the gene expression of *p53*, *Bax*, *Casp 3*, and *Casp 9*, whereas *BCL-2* was downregulated via the intrinsic mitochondrial pathway. Our findings exposed the possibility of a future study to identify the potential therapeutic agents from *Aquilaria* species for the development of herbal-based medicine for anti-inflammatory, antioxidant, and anti-cancer after animal tests and clinical trials. Future perspective: Even though these species of plants are proven to have more medicinal properties and are precious to humankind, still this particular species is listed in the “critically endangered category”, which should be carefully considered and conserved before it is completely extinct.

Supplementary Materials: The following supporting information can be downloaded at: <https://www.mdpi.com/article/10.3390/app13106321/s1>, Table S1: predicted biological activity of Gmelofuran; Table S2: predicted biological activity of Agarol; Table S3: predicted biological activity of Aquillochin; Table S4: predicted biological activity of Agarospirol; Table S5: parameters evaluated for drug-likeness of Grewin and the control drug BDA-366; Table S6: parameters evaluated for absorption of Grewin and the control drug BDA-366; Table S7: parameters evaluated for distribution of Grewin and the control drug BDA-366; Table S8: parameters evaluated for the metabolism of Grewin and the control drug BDA-366; Table S9: parameters evaluated for excretion of Grewin and the control drug BDA-366; Table S10: parameters evaluated for toxicity of Grewin and the control drug BDA-366; Table S11: primer sequences used in qRT-PCR to analyze the expression of mRNA.

Author Contributions: Conceptualization, D.C.Y., D.U.Y. and S.-K.J.; methodology, J.N., V.B., M.A., A.K.V., M.N.M., M.M., R.A.; software, J.N., M.M., V.B., M.N.M., A.K.V., R.A.; validation, E.J.R., D.C.Y. and R.M.; formal analysis, J.N., R.M. and M.A.; resources, D.C.Y., D.U.Y. and S.-K.J.; data curation, E.J.R., J.N. and R.A.; writing—original draft preparation, J.N., E.J.R. and V.B.; writing—review and editing, J.N., E.J.R., V.B., R.M. and D.C.Y.; supervision, D.C.Y., D.U.Y. and S.-K.J.; project administration, R.M., D.C.Y., D.U.Y. and S.-K.J.; funding acquisition, D.C.Y., D.U.Y. and S.-K.J. All authors have read and agreed to the published version of the manuscript.

Funding: This work was supported by the Korea Institute of Planning and Evaluation for Technology in Food, Agriculture and Forestry (IPET) through the Agri-food Export Business Model Development Program, funded by the Ministry of Agriculture, Food and Rural Affairs (MAFRA) (Project No: 320104-03). The grant is also supported by the Nature Garden, South Korea.

Institutional Review Board Statement: Not applicable.

Informed Consent Statement: The human lung cancer cell was collected from cell bank Korea and was previously used for various research related to lung cancer at Kyung Hee University at Hanbang bio lab.

Data Availability Statement: The data that support the findings of this study are included in the Supplementary Files.

Conflicts of Interest: The authors declare no conflict of interest.

References

1. Woldesellassie, M.; Eyasu, M.; Kelbessa, U. In vivo anti-inflammatory activities of leaf extracts of *Ocimum lamifolium* in mice model. *J. Ethnopharmacol.* **2011**, *134*, 32–36. [[CrossRef](#)]
2. Rasheed, H. Studies of Oxygenation-1 (cox-1) and Oxygenation (cox-2) Inhibitors with Analgesic, Anti-Inflammatory and Anti-platelet Activities. Ph. D. Thesis, University of Karachi Pakistan, Karachi, Pakistan, 2003.
3. Sung, H.; Ferlay, J.; Siegel, R.L.; Laversanne, M.; Soerjomataram, I.; Jemal, A.; Bray, F. Global cancer statistics 2020: GLOBOCAN estimates of incidence and mortality worldwide for 36 cancers in 185 countries. *CA Cancer J. Clin.* **2021**, *71*, 209–249. [[CrossRef](#)]
4. Miller, K.D.; Nogueira, L.; Mariotto, A.B.; Rowland, J.H.; Yabroff, K.R.; Alfano, C.M.; Jemal, A.; Kramer, J.L.; Siegel, R.L. Cancer treatment and survivorship statistics, 2019. *CA Cancer J. Clin.* **2019**, *69*, 363–385. [[CrossRef](#)]

5. Ettinger, D.S.; Wood, D.E.; Aggarwal, C.; Aisner, D.L.; Akerley, W.; Bauman, J.R.; Bharat, A.; Bruno, D.S.; Chang, J.Y.; Chirieac, L.R. NCCN guidelines insights: Non-small cell lung cancer, version 1.2020: Featured updates to the NCCN guidelines. *JNCCN J. Natl. Compr. Cancer Netw.* **2019**, *17*, 1464–1472. [[CrossRef](#)] [[PubMed](#)]
6. Keklikoglou, I.; Cianciaruso, C.; Güç, E.; Squadrito, M.L.; Spring, L.M.; Tazzyman, S.; Lambein, L.; Poissonnier, A.; Ferraro, G.B.; Baer, C. Chemotherapy elicits pro-metastatic extracellular vesicles in breast cancer models. *Nat. Cell Biol.* **2019**, *21*, 190–202. [[CrossRef](#)] [[PubMed](#)]
7. Dixit, S.; Ali, H. Anticancer activity of medicinal plant extract—a review. *J. Chem. Chem. Sci.* **2010**, *1*, 79–85.
8. Azab, A.; Nassar, A.; Azab, A.N. Anti-inflammatory activity of natural products. *Molecules* **2016**, *21*, 1321. [[CrossRef](#)] [[PubMed](#)]
9. International Expert Meeting on the Treatment of SbTCM; The Integration of Traditional Chinese Medicine with Western Medicine. SARS: Clinical trials on treatment using a combination of traditional Chinese medicine and Western medicine. In Proceedings of the Report of the WHO International Expert Meeting to Review and Analyse Clinical Reports on Combination Treatment for SARS, Beijing, China, 8–10 October 2003.
10. Millaty, I.; Wijayanti, N.; Hidayati, L.; Nuringtyas, T. Identification of anticancer compounds in leaves extracts of agarwood (*Aquilaria malaccensis* (Lamk.)). In *IOP Conference Series: Earth and Environmental Science*; IOP Publishing: Bristol, UK, 2020; p. 012036.
11. Tilburt, J.C.; Kaptchuk, T.J. Herbal medicine research and global health: An ethical analysis. *Bull. World Health Organ.* **2008**, *86*, 594–599. [[CrossRef](#)]
12. World Health Organization. Programme on Traditional, M. In *WHO Traditional Medicine Strategy 2002–2005*; World Health Organization: Geneva, Switzerland, 2002.
13. Tan, C.S.; Isa, N.M.; Ismail, I.; Zainal, Z. Agarwood induction: Current developments and future perspectives. *Front. Plant Sci.* **2019**, *10*, 122. [[CrossRef](#)]
14. Wang, S.; Yu, Z.; Wang, C.; Wu, C.; Guo, P.; Wei, J. Chemical constituents and pharmacological activity of agarwood and *Aquilaria* plants. *Molecules* **2018**, *23*, 342. [[CrossRef](#)]
15. Lee, S.Y.; Mohamed, R. The origin and domestication of *Aquilaria*, an important agarwood-producing genus. In *Agarwood: Science Behind the Fragrance*; Springer: Berlin/Heidelberg, Germany, 2016; pp. 1–20.
16. Persoon, G.A.; van Beek, H.H. Growing ‘the wood of the gods’: Agarwood production in southeast Asia. In *Smallholder Tree Growing for Rural Development and Environmental Services*; Springer: Berlin/Heidelberg, Germany, 2008; pp. 245–262.
17. Eissa, M.A.; Hashim, Y.Z.-Y.; Salleh, H.M.; Abd-Azziz, S.S.; Isa, M.L.M.; Abd Warif, N.M.; Nor, Y.A.; El-Kersh, D.M.; Sani, S.A. *Aquilaria* species as potential anti-inflammatory agents—A review on in vitro and in vivo studies. *Indian J. Nat. Prod. Resour.* **2020**, *11*, 141–154.
18. Zulkifle, N. *Antidiabetic Activity of Aquilaria malaccensis (Agarwood) Leaves Extracts*; University Malaysia Pahang Gambang: Pahang, Malaysia, 2018.
19. Chitre, T.; Bhutada, P.; Nandakumar, K.; Somani, R.; Miniyar, P.; Mundhada, Y.; Gore, S.; Jain, K.J.P.O. Analgesic and anti-inflammatory activity of heartwood of *Aquilaria agallocha* in laboratory animals. *Pharmacologyonline* **2007**, *1*, 288–298.
20. Yadav, D.K.; Mudgal, V.; Agrawal, J.; Maurya, A.K.; Bawankule, D.U.; Chanotiya, C.S.; Khan, F.; Thul, S.T. Molecular docking and ADME studies of natural compounds of Agarwood oil for topical anti-inflammatory activity. *Curr. Comput.-Aided Drug Des.* **2013**, *9*, 360–370. [[CrossRef](#)]
21. Jin, Y.; Huynh, D.T.N.; Myung, C.-S.; Heo, K.-S. Ginsenoside Rh1 Prevents Migration and Invasion through Mitochondrial ROS-Mediated Inhibition of STAT3/NF- κ B Signaling in MDA-MB-231 Cells. *Int. J. Mol. Sci.* **2021**, *22*, 10458. [[CrossRef](#)] [[PubMed](#)]
22. Yang, Y.; Karakhanova, S.; Hartwig, W.; D’Haese, J.G.; Philippov, P.P.; Werner, J.; Bazhin, A.V. Mitochondria and mitochondrial ROS in cancer: Novel targets for anticancer therapy. *J. Cell. Physiol.* **2016**, *231*, 2570–2581. [[CrossRef](#)] [[PubMed](#)]
23. Wang, Y.; Qi, H.; Liu, Y.; Duan, C.; Liu, X.; Xia, T.; Chen, D.; Piao, H.-L.; Liu, H.-X. The double-edged roles of ROS in cancer prevention and therapy. *Theranostics* **2021**, *11*, 4839. [[CrossRef](#)] [[PubMed](#)]
24. Chakraborty, S.; Mazumdar, M.; Mukherjee, S.; Bhattacharjee, P.; Adhikary, A.; Manna, A.; Chakraborty, S.; Khan, P.; Sen, A.; Das, T. Restoration of p53/miR-34a regulatory axis decreases survival advantage and ensures Bax-dependent apoptosis of non-small cell lung carcinoma cells. *FEBS Lett.* **2014**, *588*, 549–559. [[CrossRef](#)]
25. Lu, H.-F.; Chie, Y.-J.; Yang, M.-S.; Lee, C.-S.; Fu, J.-J.; Yang, J.-S.; Tan, T.-W.; Wu, S.-H.; Ma, Y.-S.; Ip, S.-W. Apigenin induces caspase-dependent apoptosis in human lung cancer A549 cells through Bax-and Bcl-2-triggered mitochondrial pathway. *Int. J. Oncol.* **2010**, *36*, 1477–1484.
26. Wang, J.-P.; Hsieh, C.-H.; Liu, C.-Y.; Lin, K.-H.; Wu, P.-T.; Chen, K.-M.; Fang, K. Reactive oxygen species-driven mitochondrial injury induces apoptosis by teroxirone in human non-small cell lung cancer cells. *Oncol. Lett.* **2017**, *14*, 3503–3509. [[CrossRef](#)]
27. Piao, M.J.; Yoo, E.S.; Koh, Y.S.; Kang, H.K.; Kim, J.; Kim, Y.J.; Kang, H.H.; Hyun, J.W. Antioxidant effects of the ethanol extract from flower of *Camellia japonica* via scavenging of reactive oxygen species and induction of antioxidant enzymes. *Int. J. Mol. Sci.* **2011**, *12*, 2618–2630. [[CrossRef](#)]
28. Vertuani, S.; Angusti, A.; Manfredini, S. The antioxidants and pro-antioxidants network: An overview. *Curr. Pharm. Des.* **2004**, *10*, 1677–1694. [[CrossRef](#)] [[PubMed](#)]
29. Juráňová, J.; Franková, J.; Ulrichová, J. The role of keratinocytes in inflammation. *J. Appl. Biomed.* **2017**, *15*, 169–179. [[CrossRef](#)]

30. Hu, T.-Y.; Ju, J.-M.; Mo, L.-H.; Ma, L.; Hu, W.-H.; You, R.-R.; Chen, X.-Q.; Chen, Y.-Y.; Liu, Z.-Q.; Qiu, S.-Q. Anti-inflammation action of xanthenes from *Swertia chirayita* by regulating COX-2/NF- κ B/MAPKs/Akt signaling pathways in RAW 264.7 macrophage cells. *Phytomedicine* **2019**, *55*, 214–221. [[CrossRef](#)] [[PubMed](#)]
31. Wang, H.M.-D.; Fu, L.; Cheng, C.C.; Gao, R.; Lin, M.Y.; Su, H.L.; Belinda, N.E.; Nguyen, T.H.; Lin, W.-H.; Lee, P.C. Inhibition of LPS-induced oxidative damages and potential anti-inflammatory effects of *Phyllanthus emblica* extract via down-regulating NF- κ B, COX-2, and iNOS in RAW 264.7 cells. *Antioxidants* **2019**, *8*, 270. [[CrossRef](#)]
32. Ali, M.B.; Hahn, E.J.; Paek, K.-Y. CO₂-induced total phenolics in suspension cultures of *Panax ginseng* CA Mayer roots: Role of antioxidants and enzymes. *Plant Physiol. Biochem.* **2005**, *43*, 449–457. [[CrossRef](#)]
33. Tristantini, D.; Amalia, R. Quercetin concentration and total flavonoid content of anti-atherosclerotic herbs using aluminum chloride colorimetric assay. In *Proceedings of the AIP Conference Proceedings*; AIP Publishing LLC: College Park, MD, USA, 2019; p. 030012.
34. Su, Y.; Li, L. Structural characterization and antioxidant activity of polysaccharide from four auriculariales. *Carbohydr. Polym.* **2020**, *229*, 115407. [[CrossRef](#)]
35. Bhalodia, N.R.; Nariya, P.B.; Acharya, R.; Shukla, V. In vitro antioxidant activity of hydro alcoholic extract from the fruit pulp of *Cassia fistula* Linn. *Ayu* **2013**, *34*, 209. [[CrossRef](#)]
36. Singh, D.; Gawande, D.Y.; Singh, T.; Poroikov, V.; Goel, R.K. Revealing pharmacodynamics of medicinal plants using *in silico* approach: A case study with wet lab validation. *Comput. Biol. Med.* **2014**, *47*, 1–6. [[CrossRef](#)]
37. Xiong, G.; Wu, Z.; Yi, J.; Fu, L.; Yang, Z.; Hsieh, C.; Yin, M.; Zeng, X.; Wu, C.; Lu, A. ADMETlab 2.0: An integrated online platform for accurate and comprehensive predictions of ADMET properties. *Nucleic Acids Res.* **2021**, *49*, W5–W14. [[CrossRef](#)]
38. Souers, A.J.; Levenson, J.D.; Boghaert, E.R.; Ackler, S.L.; Catron, N.D.; Chen, J.; Dayton, B.D.; Ding, H.; Enschede, S.H.; Fairbrother, W.J. ABT-199, a potent and selective BCL-2 inhibitor, achieves antitumor activity while sparing platelets. *Nat. Med.* **2013**, *19*, 202–208. [[CrossRef](#)]
39. Vainer, R.; Cohen, S.; Shahar, A.; Zarivach, R.; Arbely, E. Structural basis for p53 Lys120-acetylation-dependent DNA-binding mode. *J. Mol. Biol.* **2016**, *428*, 3013–3025. [[CrossRef](#)] [[PubMed](#)]
40. Garner, T.P.; Reyna, D.E.; Priyadarshi, A.; Chen, H.-C.; Li, S.; Wu, Y.; Ganesan, Y.T.; Malashkevich, V.N.; Cheng, E.H.; Gavathiotis, E. An autoinhibited dimeric form of BAX regulates the BAX activation pathway. *Mol. Cell* **2016**, *63*, 485–497. [[CrossRef](#)] [[PubMed](#)]
41. Maciag, J.J.; Mackenzie, S.H.; Tucker, M.B.; Schipper, J.L.; Swartz, P.; Clark, A.C. Tunable allosteric library of caspase-3 identifies coupling between conserved water molecules and conformational selection. *Proc. Natl. Acad. Sci. USA* **2016**, *113*, E6080–E6088. [[CrossRef](#)]
42. Chao, Y.; Shiozaki, E.N.; Srinivasula, S.M.; Rigotti, D.J.; Fairman, R.; Shi, Y. Engineering a dimeric caspase-9: A re-evaluation of the induced proximity model for caspase activation. *PLoS Biol.* **2005**, *3*, e183. [[CrossRef](#)]
43. Cosconati, S.; Forli, S.; Perryman, A.L.; Harris, R.; Goodsell, D.S.; Olson, A.J. Virtual screening with AutoDock: Theory and practice. *Expert Opin. Drug Discov.* **2010**, *5*, 597–607. [[CrossRef](#)] [[PubMed](#)]
44. Trott, O.; Olson, A.J. Software news and update AutoDock Vina: Improving the speed and accuracy of docking with a new scoring function, efficient optimization, and multithreading. *J. Comput. Chem.* **2010**, *31*, 455–461.
45. Karpagam, V.; Sathishkumar, N.; Sathiyamoorthy, S.; Rasappan, P.; Shila, S.; Kim, Y.-J.; Yang, D.-C. Identification of BACE1 inhibitors from *Panax ginseng* saponins—An *In silico* approach. *Comput. Biol. Med.* **2013**, *43*, 1037–1044. [[CrossRef](#)]
46. Shrestha, S.; Natarajan, S.; Park, J.-H.; Lee, D.-Y.; Cho, J.-G.; Kim, G.-S.; Jeon, Y.-J.; Yeon, S.-W.; Yang, D.-C.; Baek, N.-I. Potential neuroprotective flavonoid-based inhibitors of CDK5/p25 from *Rhus parviflora*. *Bioorg. Med. Chem. Lett.* **2013**, *23*, 5150–5154. [[CrossRef](#)]
47. Van Der Spoel, D.; Lindahl, E.; Hess, B.; Groenhof, G.; Mark, A.E.; Berendsen, H. GROMACS: Fast, flexible, and free. *J. Comput. Chem.* **2005**, *26*, 1701–1718. [[CrossRef](#)]
48. Schüttelkopf, A.W.; Van Aalten, D.M.F. PRODRG: A tool for high-throughput crystallography of protein-ligand complexes. *Acta Crystallogr. Sect. D Biol. Crystallogr.* **2004**, *60*, 1355–1363. [[CrossRef](#)]
49. Ljungh, A.; Moran, A.P.; Wadström, T. Interactions of bacterial adhesins with extracellular matrix and plasma proteins: Pathogenic implications and therapeutic possibilities. *FEMS Immunol. Med. Microbiol.* **1996**, *16*, 117–126. [[CrossRef](#)]
50. Christen, M.; Hünenberger, P.H.; Bakowies, D.; Baron, R.; Bürgi, R.; Geerke, D.P.; Heinz, T.N.; Kastenholz, M.A.; Kräutler, V.; Oostenbrink, C.; et al. The GROMOS software for biomolecular simulation: GROMOS05. *J. Comput. Chem.* **2005**, *26*, 1719–1751. [[CrossRef](#)] [[PubMed](#)]
51. Sathishkumar, N.; Sathiyamoorthy, S.; Ramya, M.; Yang, D.U.; Lee, H.N.; Yang, D.C. Molecular docking studies of anti-apoptotic BCL-2, BCL-XL, and MCL-1 proteins with ginsenosides from *Panax ginseng*. *J. Enzym. Inhib. Med. Chem.* **2012**, *27*, 685–692. [[CrossRef](#)] [[PubMed](#)]
52. Bak, M.-J.; Jun, M.; Jeong, W.-S. Antioxidant and hepatoprotective effects of the red ginseng essential oil in H₂O₂-treated HepG2 cells and CCl₄-treated mice. *Int. J. Mol. Sci.* **2012**, *13*, 2314–2330. [[CrossRef](#)]
53. Sikdar, S.; Lallemand, B.; Dubois, J. Induction of phase II enzymes glutathione-s-transferase and NADPH: Quinone oxydoreductase 1 with novel sulfuraphane derivatives in human keratinocytes: Evaluation of the intracellular GSH level. *Pharmacol. Pharm.* **2014**, *5*, 937. [[CrossRef](#)]

54. Saeed, N.; Khan, M.R.; Shabbir, M. Antioxidant activity, total phenolic and total flavonoid contents of whole plant extracts *Torilis leptophylla* L. *BMC Complement. Altern. Med.* **2012**, *12*, 221. [[CrossRef](#)] [[PubMed](#)]
55. Aggarwal, B.B.; Shishodia, S. Molecular targets of dietary agents for prevention and therapy of cancer. *Biochem. Pharmacol.* **2006**, *71*, 1397–1421. [[CrossRef](#)]
56. Okwu, D.; Ekeke, O. Phytochemical screening and mineral composition of chewing sticks in South Eastern Nigeria. *Glob. J. Pure Appl. Sci.* **2003**, *9*, 235–238. [[CrossRef](#)]
57. Petti, S.; Scully, C. Polyphenols, oral health and disease: A review. *J. Dent.* **2009**, *37*, 413–423. [[CrossRef](#)]
58. Poroikov, V.V.; Filimonov, D.A.; Ihlenfeldt, W.D.; Glorizova, T.A.; Lagunin, A.A.; Borodina, Y.V.; Stepanchikova, A.V.; Nicklaus, M.C. PASS biological activity spectrum predictions in the enhanced open NCI database browser. *J. Chem. Inf. Comput. Sci.* **2003**, *43*, 228–236. [[CrossRef](#)]
59. Assaf, A.M.; Haddadin, R.N.; Aldouri, N.A.; Alabbassi, R.; Mashallah, S.; Mohammad, M.; Bustanji, Y.J. Anti-cancer, anti-inflammatory and anti-microbial activities of plant extracts used against hematological tumors in traditional medicine of Jordan. *J. Ethnopharmacol.* **2013**, *145*, 728–736. [[CrossRef](#)] [[PubMed](#)]
60. Khlifi, D.; Sghaier, R.M.; Amouri, S.; Laouini, D.; Hamdi, M.; Bouajila, J. Composition and anti-oxidant, anti-cancer and anti-inflammatory activities of *Artemisia herba-alba*, *Ruta chalapensis* L. and *Peganum harmala* L. *Food Chem. Toxicol.* **2013**, *55*, 202–208. [[CrossRef](#)] [[PubMed](#)]
61. Amaral, S.; Mira, L.; Nogueira, J.; da Silva, A.P.; Florêncio, M.H. Plant extracts with anti-inflammatory properties—A new approach for characterization of their bioactive compounds and establishment of structure–antioxidant activity relationships. *Food Chem. Toxicol.* **2009**, *17*, 1876–1883. [[CrossRef](#)]
62. Zou, Z.; Chang, H.; Li, H.; Wang, S.J.A. Induction of reactive oxygen species: An emerging approach for cancer therapy. *Apoptosis* **2017**, *22*, 1321–1335. [[CrossRef](#)] [[PubMed](#)]
63. Rao, P.C.; Begum, S.; Sahai, M.; Sriram, D.S. Coptisine-induced cell cycle arrest at G2/M phase and reactive oxygen species–dependent mitochondria-mediated apoptosis in non-small-cell lung cancer A549 cells. *Tumor Biol.* **2017**, *39*, 1010428317694565. [[CrossRef](#)]
64. Zaidieh, T.; Smith, J.R.; Ball, K.E.; An, Q. ROS as a novel indicator to predict anticancer drug efficacy. *BMC Cancer* **2019**, *19*, 1224. [[CrossRef](#)]
65. Zhang, J.; Wang, X.; Vikash, V.; Ye, Q.; Wu, D.; Liu, Y.; Dong, W. ROS and ROS-mediated cellular signaling. *Oxidative Med. Cell. Longev.* **2016**, *2016*, 4350965. [[CrossRef](#)]
66. Perillo, B.; Di Donato, M.; Pezone, A.; Di Zazzo, E.; Giovannelli, P.; Galasso, G.; Castoria, G.; Migliaccio, A. ROS in cancer therapy: The bright side of the moon. *Exp. Mol. Med.* **2020**, *52*, 192–203. [[CrossRef](#)]
67. Nakamura, H.; Takada, K. Reactive oxygen species in cancer: Current findings and future directions. *Cancer Sci.* **2021**, *112*, 3945–3952. [[CrossRef](#)]
68. Snezhkina, A.V.; Kudryavtseva, A.V.; Kardymon, O.L.; Savvateeva, M.V.; Melnikova, N.V.; Krasnov, G.S.; Dmitriev, A.A. ROS generation and antioxidant defense systems in normal and malignant cells. *Oxidative Med. Cell. Longev.* **2019**, *2019*, 6175804. [[CrossRef](#)]
69. Huynh, D.T.N.; Jin, Y.; Myung, C.-S.; Heo, K.-S. Ginsenoside Rh1 induces MCF-7 cell apoptosis and autophagic cell death through ROS-mediated Akt signaling. *Cancers* **2021**, *13*, 1892. [[CrossRef](#)] [[PubMed](#)]
70. Zamzami, N.; Marchetti, P.; Castedo, M.; Decaudin, D.; Macho, A.; Hirsch, T.; Susin, S.A.; Petit, P.X.; Mignotte, B.; Kroemer, G. Sequential reduction of mitochondrial transmembrane potential and generation of reactive oxygen species in early programmed cell death. *J. Exp. Med.* **1995**, *182*, 367–377. [[CrossRef](#)] [[PubMed](#)]
71. Guo, R.; Chen, X.; Nguyen, T.; Chai, J.; Gao, Y.; Wu, J.; Li, J.; Abdel-Rahman, M.A.; Chen, X.; Xu, X. The Strong Anti-Tumor Effect of Smp24 in Lung Adenocarcinoma A549 Cells Depends on Its Induction of Mitochondrial Dysfunctions and ROS Accumulation. *Toxins* **2022**, *14*, 590. [[CrossRef](#)]
72. Dai, C.-Q.; Luo, T.-T.; Luo, S.-C.; Wang, J.-Q.; Wang, S.-M.; Bai, Y.-H.; Yang, Y.-L.; Wang, Y.-Y. p53 and mitochondrial dysfunction: Novel insight of neurodegenerative diseases. *J. Bioenerg. Biomembr.* **2016**, *48*, 337–347. [[CrossRef](#)] [[PubMed](#)]
73. Knott, A.B.; Bossy-Wetzel, E. Nitric oxide in health and disease of the nervous system. *Antioxid. Redox Signal.* **2009**, *11*, 541–553. [[CrossRef](#)]
74. Korhonen, R.; Lahti, A.; Kankaanranta, H.; Moilanen, E. Nitric oxide production and signaling in inflammation. *Curr. Drug Targets-Inflamm. Allergy* **2005**, *4*, 471–479. [[CrossRef](#)] [[PubMed](#)]
75. Wang, Z.; Liu, X.; Bao, Y.; Wang, X.; Zhai, J.; Zhan, X.; Zhang, H. Characterization and anti-inflammation of a polysaccharide produced by *Chaetomium globosum* CGMCC 6882 on LPS-induced RAW 264.7 cells. *Carbohydr. Polym.* **2021**, *251*, 117129. [[CrossRef](#)] [[PubMed](#)]
76. Sahai, E. Mechanisms of cancer cell invasion. *Curr. Opin. Genet. Dev.* **2005**, *15*, 87–96. [[CrossRef](#)]
77. Johnson, T.M.; Yu, Z.-X.; Ferrans, V.J.; Lowenstein, R.A.; Finkel, T. Reactive oxygen species are downstream mediators of p53-dependent apoptosis. *Proc. Natl. Acad. Sci. USA* **1996**, *93*, 11848–11852. [[CrossRef](#)]
78. Liu, B.; Chen, Y.; Clair, D.K.S. ROS and p53: A versatile partnership. *Free Radic. Biol. Med.* **2008**, *44*, 1529–1535. [[CrossRef](#)]
79. Aubrey, B.J.; Kelly, G.L.; Janic, A.; Herold, M.J.; Strasser, A. How does p53 induce apoptosis and how does this relate to p53-mediated tumour suppression? *Cell Death Differ.* **2018**, *25*, 104–113. [[CrossRef](#)] [[PubMed](#)]

80. Li, Y.; Wang, Y.; Yu, X.; Yu, T.; Zheng, X.; Chu, Q. *Radix tetragtisma* inhibits the non-small cell lung cancer via Bax/Bcl-2/Caspase-9/Caspase-3 pathway. *Nutr. Cancer* **2022**, *74*, 320–332. [[CrossRef](#)] [[PubMed](#)]
81. Cao, J.; Naeem, M.; Noh, J.-K.; Lee, E.H.; Yoo, J.-W. Dexamethasone phosphate-loaded folate-conjugated polymeric nanoparticles for selective delivery to activated macrophages and suppression of inflammatory responses. *Macromol. Res.* **2015**, *23*, 485–492. [[CrossRef](#)]
82. Yang, M.; Wang, Y.; Patel, G.; Xue, Q.; Njateng, G.S.S.; Cai, S.; Cheng, G.; Kai, G. In vitro and in vivo anti-inflammatory effects of different extracts from *Epigynum auritum* through down-regulation of NF- κ B and MAPK signaling pathways. *J. Ethnopharmacol.* **2020**, *261*, 113105. [[CrossRef](#)] [[PubMed](#)]
83. Huang, H.; Hu, G.; Wang, C.; Xu, H.; Chen, X.; Qian, A. Cepharanthine, an alkaloid from *Stephania cepharantha* Hayata, inhibits the inflammatory response in the RAW264. 7 cell and mouse models. *Inflammation* **2014**, *37*, 235–246. [[CrossRef](#)]
84. Alscher, R.G.; Erturk, N.; Heath, L.S. Role of superoxide dismutases (SODs) in controlling oxidative stress in plants. *J. Exp. Bot.* **2002**, *53*, 1331–1341. [[CrossRef](#)]

Disclaimer/Publisher’s Note: The statements, opinions and data contained in all publications are solely those of the individual author(s) and contributor(s) and not of MDPI and/or the editor(s). MDPI and/or the editor(s) disclaim responsibility for any injury to people or property resulting from any ideas, methods, instructions or products referred to in the content.